IEEE Access
Multidisciplinary ⋮ Rapid Review ⋮ Open Access Journal

Received 31 May 2023, accepted 29 June 2023, date of publication 17 July 2023, date of current version 25 July 2023.

Digital Object Identifier 10.1109/ACCESS.2023.3296100

RESEARCH ARTICLE

A Real-Time Control System of Upper-Limb Human Musculoskeletal Model With Environmental Integration

AZHAR AULIA SAPUTRA[1], (Member, IEEE), CHIN WEI HONG[1], TADAMITSU MATSUDA[2], (Member, IEEE), AND NAOYUKI KUBOTA[1], (Senior Member, IEEE)

[1]Department of Mechanical Systems Engineering, Graduate School of System Design, Tokyo Metropolitan University, Hino, Tokyo 191-0065, Japan
[2]Faculty of Health Sciences, Department of Physical Therapy, Juntendo University, Bunkyo-ku, Tokyo 113-0033, Japan

Corresponding authors: Azhar Aulia Saputra (aa.saputra@tmu.ac.jp) and Naoyuki Kubota (kubota@tmu.ac.jp)

This work was supported by in part by the Japan Science and Technology Agency (JST) (Moonshot RnD) under Grant JP-MJMS2034.

This work involved human subjects or animals in its research. Approval of all ethical and experimental procedures and protocols was granted by the Tokyo Metropolitan University Review Board under Approval No. H21-051.

ABSTRACT The intricate dynamics of the human musculoskeletal system require complex mathematical computations for accurate simulation, posing challenges in estimating muscle activity. Real-time processes and comprehensive analysis greatly influence the effectiveness of monitoring applications. The objective of our research was to enhance real-time muscle activity predictions by incorporating environmental data into human musculoskeletal simulations, focusing on the upper extremity. Our model, developed using MuJoCo software, consisted of 50 Hill-type muscles and integrated environmental context. Information on human posture was collected from single RGBD sensors positioned at 32 three-dimensional node locations. We used inverse kinematics computations to convert this data into joint angle parameters for our simulation model. The stretch reflex of each muscle was regulated to initiate movement in the target joints. Desired muscle stretch length was derived from the mechanical interaction between the bone structure and the muscle-tendon actuator connected to it. Our model also allowed for the application of artificial force to simulate external load conditions. To validate our model, we performed basic movements with the upper extremity and measured muscle activity using EMG sensors. Our results confirmed the model's ability to accurately predict muscle activation and the force exerted by each muscle. Further experiments demonstrated its potential for seamless integration with dynamic environmental conditions, thereby enhancing its utility as a comprehensive human physical monitoring system.

INDEX TERMS Musculoskeletal model, upper extremity, real-time muscle-activity estimation.

I. INTRODUCTION

Computational musculoskeletal simulations are frequently used to assess muscles' function during movement and examine the consequences of changes in the musculoskeletal system or its neurological control caused by age, gender, injury, disease, or clinical interventions. It can be difficult or impossible to determine the contributions of individual muscles experimentally due to the complexity and multi-joint arrangements of many muscles as well as the large numbers of muscles coordinated during a single movement. Computer modelling allows scientists to explore the database of quantitative anatomy embodied in biomechanical models to identify the contributions of individual muscles to a movement of interest by combining anatomical information about the size and arrangement of muscles and segments in a system with information about the pattern of muscle activation during movement [1].

The associate editor coordinating the review of this manuscript and approving it for publication was Xiaogang Jin.

There are many simulations of human musculoskeletal models which are conceptually similar to each other [2], [3], [4], [5], [6]. They use human musculoskeletal with Hill-type muscle models [7], [8], while other simulations have been developed for animal musculoskeletal models [6], [9]. Delp et al., (some of the researchers who developed a Hill-type-muscle model), made their model interactive so that it could examine the effects of various pathologies on the human musculoskeletal system. Saul et al. [4], have developed an upper-limb musculoskeletal model. Holzbaur et al. has also presented an upper-limb extremity model [10]. These models have all been validated for biological fidelity.

These achievements provide insight applicable to monitoring the muscle activity of humans. For example, the models can be utilized for seamless muscle-strength detection, replacing the current method of muscle strength measurements that requires a second person (for example, the caregiver) to take the measurement [11]. This may also open an opportunity between patient and caregiver to engage with biomechanical data in real-time during a patient examination [12]. By decreasing the time required for data acquisition, this monitoring system also reduces the cost. However, this kind of target requires real-time musculoskeletal processing.

Creating a real-time human musculoskeletal model requires real-time human muscle activation analysis based on measured human pose recognition. It can bridge the gap between data gathering and quick muscle analysis. Several methods have been used to achieve the real-time human musculoskeletal model [13], [14], [15], [16], [17]. Some of them consider joint moment analysis without the muscle-activity variable [18], [19]. This method employs synthetic simulation signals rather than accurate muscle actuator analysis. Furthermore, the model is evaluated on a desktop computer with associated computing performance and lacks the ability to forecast internal joint forces accurately. The issue of biological fidelity of real-time muscle analysis has also been found in some current research [15] because is required to achieve accurate human muscle analysis. Durandau et al. developed a real-time lower-extremity musculoskeletal modeling pipeline driven by data from EMG and motion-capture using the OpenSim platform [13], [20]. However, this model needs an EMG signal to measure muscle activation.

Real-time human muscle monitoring requires integrating feedback of force measurements from external sensors. Muscle monitoring uses several methods, each testing a different measurement of strength. Isometric, isokinetic, and isoinertial strength measurements all have different reliabilities [11]. For example, the isometric test involves generating a static force while the length of the muscle remains relatively constant. The test requires the subject to push or pull against fixed force sensors, such as the grip strength test. The force value thus generated is then used as the feedback input to the model. Limited sensory output, such as ground force sensors collisions with other objects, require a simulated environment to generate the force feedback. The muscle must generate the force to respond to the dynamic feedback input in real time.

Responding to dynamic external force input in a real-time musculoskeletal model requires an efficient muscle control mechanism. Considering the trade-off between muscle complexity and computational speed is essential to building the musculoskeletal model. The muscle actuator has been represented as torque-driven [21]. In our previous work, we have developed a muscle model of a legged animal for analyzing its gait in an Open Dynamic Engine simulation [22], [23]. We used a torque-driven mechanism to represent the muscle. This control has fast computational speed with good performance. However, it is far from being biologically accurate. The number of muscles driven also affects the computational cost in most simulation engines. On the other hand, the MuJoCo simulation engine shows prospective results in a tendon-based actuator [24]. Therefore, balancing muscle complexity and computational speed, we used MuJoCo as the basis of our physical simulation.

We propose to develop a human musculoskeletal model simulation for a real-time human physical measurement system firmly integrated with sensory feedback of environmental conditions. The proposed model considers a seamless and natural measurement system to improve users' comfort, especially that of older people. The effectiveness of the proposed model has been validated through several muscle-activity validation experiments.

- Real-time control system of human upper limb muscle activity for human physical monitoring.
- Providing real-time integration between the human musculoskeletal model with environmental conditions, acquiring feedback force from the environmental condition.

This paper is organized as follows. Section II shows the upper-limb musculoskeletal model, muscle properties, and their implementation on the proposed simulation engine MuJoCo. Section III explains the proposed real-time control system. Section IV introduces our proposed ''living lab'' that is used for the implementation of the proposed model. To validate the proposed control system, Section V illustrates several experiments. Finally, we conclude and discuss further development in Section VI.

II. UPPER-LIMB MUSCULOSKELETAL MODEL

A physics-based computer simulation is the essential framework for the human musculoskeletal model. The different calculation methods may affect the computational complexity of the model. Because we require cost-efficiency along with real-time estimation and the ability to integrate environmental feedback, efficient computational cost is essential. We therefore selected a basic physics engine as the base of our model. Many human musculoskeletal simulation models are available. Some of them are integrated with firm software

such as OpenSim [3], Anybody [25], [26], SIMM [26], MSMS [2], and MSk software [27]. Furthermore, The Delft Shoulder and Elbow Model (DSEM) built the model in SPACAR [28], [29]. The current model is able to estimate muscle activity precisely, show reliability visualization, and offers flexibility in parameter modelling. However, real-time estimation is one of the issues in those models. Flexibility of data acquisition varies with software. Lee et al. have developed a comprehensive human musculoskeletal model in a DART simulation engine [30]. However, DART is unstable when the object is small with a high damping value [31]. In contrast, MuJoCo has faster and better accuracy over a longer time looping compared with other simulations [32].

A. MUSCULOSKELETAL PROPERTIES

In the upper-limb musculoskeletal model, we modified the Saul model proposed in [4]. The joint structure, composed of 15 degrees of freedom, is based on the kinematics of the Holzbaur model [10]. It is composed of glenohumeral (clavicle and scapula) joints [33], elbow, forearm, wrist, thumb, and fingers based on the recommendation by the International Society of Biomechanics [34]. We converted the model from OpenSim to MuJoCo using [35]. However, several structural characteristics in MuJoCo are challenging to represent precisely and should be estimated. We built the joints in our hands to activate the Flexor Digitorum and Extensor Digitorum.

In biomechanics, a muscle and a tendon are connected to produce a muscle-tendon actuator. In MuJoCo, the muscle-tendon combination is given the spatial properties of the tendon. Therefore, the length of the muscle actuator L_{act} becomes the sum of muscle length (L_M) and tendon length (L_T), $L_{act} = L_M + L_T$ in this model. Instead of defining optimum tendon length L_O, we defined scaled range[0] and range[1] from the following equations:

$$range[0] = (L_{act}[0] - L_T)/L_O \tag{1}$$

and

$$range[1] = (L_{act}[1] - L_T)/L_O \tag{2}$$

To define the maximum force of each muscle actuator, we defined the force scale parameter of each muscle. The muscle-modeling parameters are tabulated in Table 1. The advantage of the scaled quantities is that all muscles behave similarly and the equations represent all situations.

B. MUSCULOSKELETAL PROPERTIES

Our muscle actuator is based on a Hill-type muscle model [38] where the total length of the muscle actuator (l^{mt}) is calculated as follows:

$$l_{mt} = l_m \cos\alpha + l_t \tag{3}$$

l_m and l_t are the length of muscle and length of the tendon, respectively. Parameter α is the pennation angle at a certain

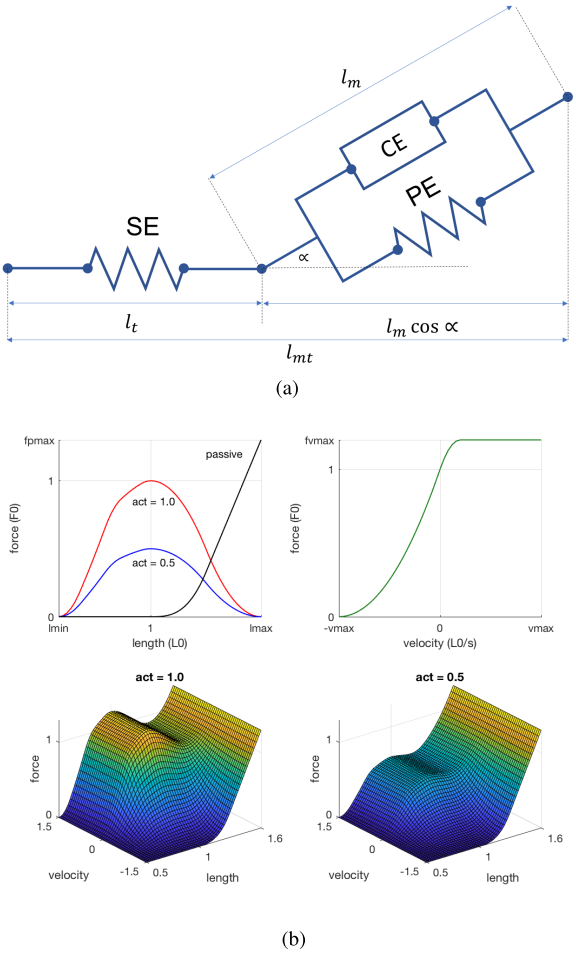

FIGURE 1. (a) Structure of hill-type muscle model (b) Diagram of force-length-velocity function.

muscle length l_m. In the current state, the pennation angle is assumed to be 0. The effect of the pennation angle can be approximated by adjusting the muscle force scale and also adjusting the operating range (range[0] and range[1]) that is defined in Table 1.

The muscle actuator model assumes the force is generated from the force-length-velocity function calculated in Equations (5),(6), and (7) shown in Fig. 1.

$$F_{TOTAL} = F_m^0(a(t)F_L(\tilde{l}_m)F_V(\tilde{v}_m) + F_P(\tilde{l}_m)) \tag{4}$$

Passive force is calculated in Equation (5), where f_{max}^p is the maximum passive force and parameter b is calculated from $b = 0.5(1 + l_{max})$. l_{min} and l_{max} is the range of muscle length. The muscle length under force is calculated in Equation (6), where the value of B is calculated in Equation (8). The force velocity of the muscle is calculated from Equation (7), where v_{max}, f_{max}^v, v are the maximum accepted muscle velocity, maximum of force muscle, and the normalized current muscle actuator velocity. Parameter v is calculated as $v = V_{act}/v_{max}$. In Equation (8), l_L is calculated as $l_L = 0.5 * (C_i + 1)$ and l_R

TABLE 1. Muscle modeling parameters.

Muscle's name	Abbrev. of muscle	Optimal Fiber Length (cm)	Maximum Isometric Force (N)	Tendon Slack Length (cm)	Mujoco Paramters				
					Actuator Length min. (cm)	Actuator Length max. (cm)	Range[0]	Range[1]	Muscle Force scale
Shoulder									
Deltoid Anterior	DELT1	9.8	1142.6	9.3	14.2	29.88	0.257	1.077	2285
Deltoid Medial	DELT2	10.8	1142.6	11	16.4	33.68	0.248	1.040	2285
Deltoid Posterior	DELT3	13.7	259.9	3.8	10.65	32.57	0.391	1.644	520
Supraspinatus	SUPSP	6.8	487.8	4	7.4	18.28	0.315	1.322	976
Infraspinatus	INFSP	7.6	1210.8	3.1	6.9	19.06	0.355	1.492	2422
Subscapularis	SUBSC	8.7	1377.8	3.3	7.65	21.57	0.363	1.523	2756
Teres minor	TMIN	7.4	354.3	7.1	10.8	22.64	0.255	1.072	709
Teres major	TMAJ	16.2	425.4	2	10.1	36.02	0.445	1.869	851
Pectoralis major Clavicular	PECM1	14.4	364.4	0.3	7.5	30.54	0.490	2.057	729
Pectoralis major Sternal	PECM2	13.8	515.4	8.9	15.8	37.88	0.304	1.277	1031
Pectoralis major Ribs	PECM3	13.8	390.5	13.2	20.1	42.18	0.256	1.073	781
Latissimus dorsi Thoracic	LAT1	25.4	389.1	12	24.7	65.34	0.340	1.426	778
Latissimus dorsi Lumbar	LAT2	23.3	389.1	17.7	29.35	66.63	0.284	1.193	778
Latissimus dorsi Iliac	LAT3	27.9	281.7	14	27.95	72.59	0.333	1.398	563
Coracobrachialis	CORB	9.3	242.5	9.7	14.35	29.23	0.245	1.028	485
Elbow									
Triceps long	TRILong	13.4	798.5	14.3	21	42.44	0.242	1.016	1597
Triceps lateral	TRILat	11.4	624.3	9.8	15.5	33.74	0.269	1.129	1249
Triceps madial	TRIMed	11.4	624.3	9.1	14.8	33.04	0.278	1.168	1249
Anconeus	ANC	2.7	350.0	1.8	3.15	7.47	0.300	1.260	700
Supinator	SUP	3.3	476.0	2.8	4.45	9.73	0.270	1.136	952
Biceps long	BICLong	11.6	624.3	27.2	33	51.56	0.149	0.628	1249
Biceps short	BICShort	13.2	435.6	19.2	25.8	46.92	0.204	0.856	871
Brachialis	BRA	8.6	987.3	5.4	9.7	23.46	0.307	1.290	1975
Brachioradialis	BRD	17.3	261.3	13.3	21.95	49.63	0.283	1.187	523
Forearm									
Extensor carpi radialis longus	ECRL	8.1	304.9	22.4	26.45	39.41	0.133	0.558	610
Extensor carpi radialis brevis	ECRB	5.9	100.5	22.2	25.15	34.59	0.105	0.441	201
Extensor carpi ulnaris	ECU	6.2	93.2	22.8	25.9	35.82	0.107	0.449	186
Flexor carpi radialis	FCR	6.3	74.0	24.4	27.55	37.63	0.103	0.431	148
Flexor carpi ulnaris	FCU	5.1	128.9	26.5	29.05	37.21	0.081	0.339	258
Palmaris longus	PL	6.4	26.7	26.9	30.1	40.34	0.096	0.404	53
Pronator teres	PT	4.9	566.2	9.8	12.25	20.09	0.167	0.700	1132
Pronator quadratus	PQ	2.8	75.5	0.5	1.9	6.38	0.424	1.782	151
Wrist/hand									
Flexor digitorum superficialis digit 5	FDSL	5.2	16.5	33.8	36.4	44.72	0.067	0.280	33
Flexor digitorum superficialis digit 4	FDSR	7.4	57.9	32.8	36.5	48.34	0.092	0.387	116
Flexor digitorum superficialis digit 3	FDSM	7.5	91.0	29.5	33.25	45.25	0.101	0.426	182
Flexor digitorum superficialis digit 2	FDSI	8.4	61.2	27.5	31.7	45.14	0.117	0.491	122
Flexor digitorum profundus digit 5	FDPL	7.5	79.7	28.2	31.95	43.95	0.105	0.441	159
Flexor digitorum profundus digit 4	FDPR	8	64.1	28.2	32.2	45	0.110	0.464	128
Flexor digitorum profundus digit 3	FDPM	8.4	81.7	29.3	33.5	46.94	0.111	0.468	163
Flexor digitorum profundus digit 2	FDPI	7.5	68.3	29.4	33.15	45.15	0.102	0.427	137
Extensor digitorum communis digit 5	EDCL	6.5	13.1	29.7	32.95	43.35	0.090	0.377	26
Extensor digitorum communis digit 4	EDCR	6.3	34.0	32.7	35.85	45.93	0.081	0.339	68
Extensor digitorum communis digit 3	EDCM	7.2	35.3	33.5	37.1	48.62	0.088	0.371	71
Extensor digitorum communis digit 2	EDCI	7	18.3	32.2	35.7	46.9	0.089	0.375	37
Extensor digiti minimi	EDM	6.8	25.3	32.3	35.7	46.58	0.087	0.365	51
Extensor indicis propius	EIP	5.9	21.7	18.6	21.55	30.99	0.120	0.506	43
Extensor pollicis longus	EPL	5.4	39.5	22.1	24.8	33.44	0.098	0.412	79
Extensor pollicis brevis	EPB	6.8	14.2	11.5	14.9	25.78	0.186	0.780	28
Flexor pollicis longus	FPL	5.5	77.2	19.4	22.15	30.95	0.110	0.464	154
Abductor pollicis longus	APL	7.1	59.5	13	16.55	27.91	0.177	0.742	119

1) The muscle properties is used reflected from Saul model [4].
2) Fiber length and pennation angle refer to the study by Holzbaur [10]
3) Peak forces and isometric force of each muscle are defined from experimental result in [36], [37]
4) Minimum and maximum of actuator length in MuJoCo paramters are defined by $L_{ACT}^{(min)} = \tilde{l}_{min} l_m^o \cos\alpha + l_t^s$ and $L_{ACT}^{(max)} = \tilde{L}_{max} l_m^o \cos\alpha + l_t^s$, where $\tilde{L}_{min}$ and $\tilde{L}_{max}$ is defined 0.4 and 1.6.

is calculated as $l_R = 0.5 * (1 + C_x)$.

$$F_P = \begin{cases} 0 & \text{if } L_{act} \leq 1.0 \\ 0.25\, f^p_{max}((L_{act} - 1)/(b - 1))^3 & \text{if } L_{act} \leq b \\ 0.25\, f^p_{max}(1 + 3((L_{act} - b)/(b - 1))) & \text{otherwise} \end{cases} \tag{5}$$

$$F_L = B(L_{act}, l_{min}, 1, l_{max}) + 0.15\, B(L_{act}, l_{min}, 0.5(l_{min} + 0.95), 0.95) \tag{6}$$

$$F_V = \begin{cases} 0 & \text{if } v \leq -1 \\ (1 + V_{act}/v_{max})^2 & \text{if } v \leq 0 \\ f^v_{max} - (f^v_{max} - 1 - v)^2/(f^v_{max} - 1) & \text{if } v \leq (f^v_{max} - 1) \\ f^v_{max} & \text{otherwise} \end{cases} \tag{7}$$

$$B(L, C_i, m, C_x) = \begin{cases} 0 & \text{if } L \leq C_i || L \geq C_x \\ 0.5((L - C_i)/(l_L - C_i))^2 & \text{if } L < l_L \\ 1 - 0.5((m - L)/(m - l_L))^2 & \text{if } L < m \\ 1 - 0.5((L - m)/(l_R - m))^2 & \text{if } L < l_R \\ 0.5((C_x - L)/(C_x - l_R))^2 & \text{otherwise} \end{cases} \tag{8}$$

In order to calculate the activation dynamics ($a(t)$), we refer to the Thelen model [39] implemented on OpenSim, which can be seen in Eqs. (9).

$$\frac{da(t)}{dt} = \frac{u(t) - a(t)}{\tau_{act}} \tag{9}$$

Parameters $u(t)$ and τ_{act} are the input of neural excitation to the muscle and the time-constant parameter, respectively. The model considers the tendon to be stiff and inextensible. The force produced by the contractile element specified equals the forces generated along the tendon (F_t), which is calculated as follow:

$$F_t = F \cos(\alpha) \tag{10}$$

III. CONTROL MODEL

There are many methodologies to control the human musculoskeletal model. To consider external environmental feedback forces, we require a continuous muscle control method. Most researchers have converted the information from human posture recognition to joint angle level using their Inverse Kinematic models [7]; however, Lee et al. use Deep Reinforcement Learning (DRL) to generate proper joint angle based on target body pose [30], [40]. OpenSim adds a residual reduction algorithm to refine the generated joint angle from IK based on dynamical consistency [7].

DRL has the potential to control muscle-based actuators [41]. Lee et al. combined Quadratic Programming and DRL to consider the complexity of muscle synergies [40]. On the other hand, Proportional Derivative control has also been used for postural control in the human musculoskeletal model [42], [43]. This model considered only proprioceptive

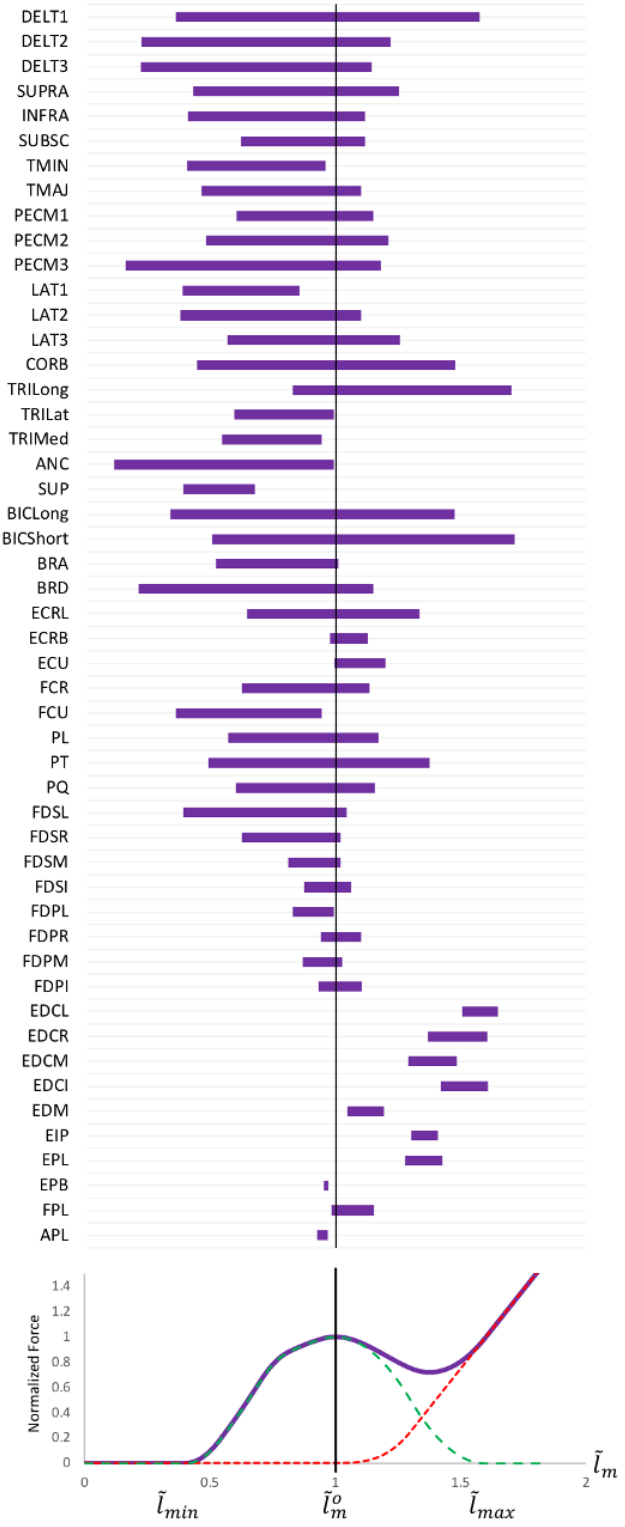

FIGURE 2. Range of normalized muscle length ($\tilde{l}_m$). The range of each muscle (l_m) (in grey span line) is acquired based on the joint movement during experimental studies.

information of muscle (muscle length and lengthening velocity). OpenSim used proportional and derivative control to track the target joint angle [7]. They successfully controlled

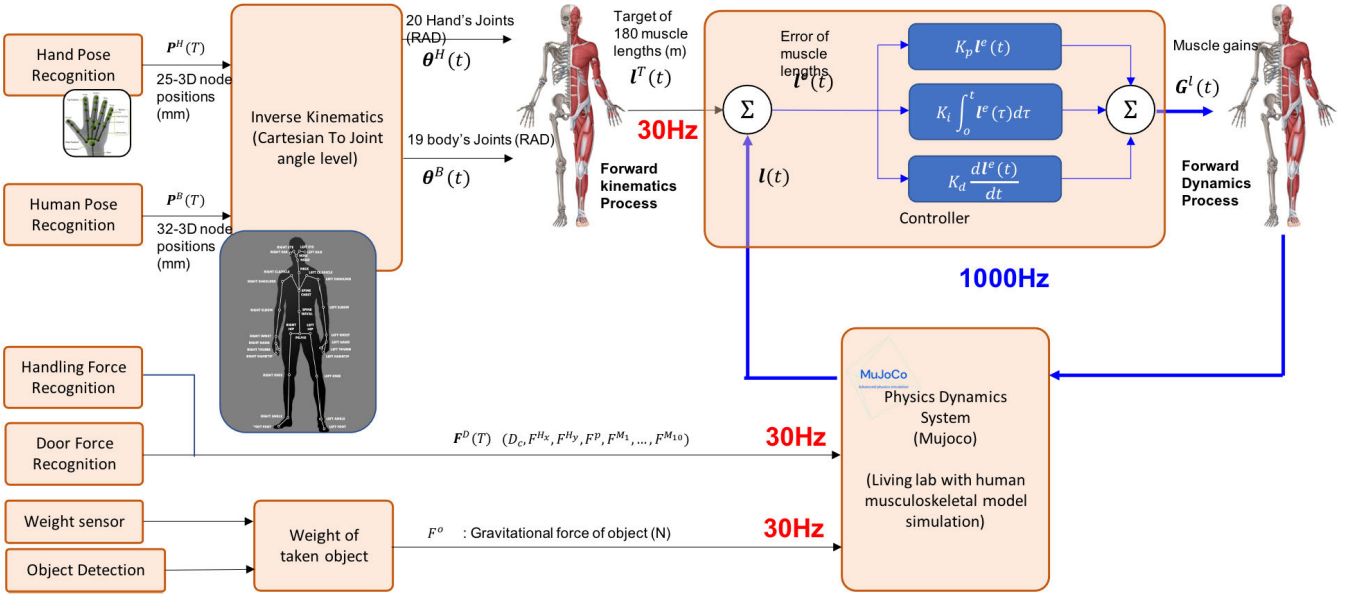

FIGURE 3. Overall control system of human musculoskeletal model. However, in the current state, we control only the upper extremity parts with 50 Hill-type muscles. Input of posture recognition: 1) P^H, 25 3D node position of hand pose 2) P^B, 25 3D node position of body pose. $\mathbf{l}^T(t)$ is the target length of muscle tendon. $\theta(t)$ and $\mathbf{l}^T(t)$ are the joint angle and the target length of muscle tendon in time t. $\mathbf{l}(T)$ and $\mathbf{l}^e(T)$ are the current length of muscle tendon and the error length of muscle tendon. Gain of muscle ($\mathbf{G}^l(t)$) is the output of the controller. The simulation also receive external force sensor which is: F^D(t) is the force recognition from door sensor, composed as D_c is the door condition, F^{Hx} is door handling force in x direction (N), F^{Hy} is door handling force in y direction (N), FP is door handling position in z direction (N), and $F^{M_1}, \ldots, F^{M_{10}}$ is force of mat sensors (N).

the model by maintaining the feedback information of muscle stretch length with efficient computation. SIMM has been confirmed in real-time process in [44]. Nevertheless, it is applied using data of pre-captured movement.

An overall-control model can be seen in Fig. 3. There are two control loops used in this proposed model, external input processed at 30 Hz and forward dynamic processed at 1000 Hz. In the external input process, posture recognition is acquired from two sensors: an RGBD Kinect camera for body pose recognition and a Leap sensor for hand pose recognition. The output of hand pose recognition is composed of 25 3D node positions (P^H), and body pose recognition is composed of 32 3D node positions (P^B). The 3D node positions are then converted to the joint angle level of the human skeletal model by the Inverse Kinematics module, explained in [45]. To obtain the change in stretched muscle length from the current joint angle, we use the Jacobian matrix to establish the relationship between quantities in joint and constraint coordinates. Once the joint angle ($\boldsymbol{\theta}(t)$) is given, we get the wrap points of muscle-tendon. To get the length of the target of the muscle actuator (l^T) from the length of the muscle-tendon wrap point, the value of (l^T) will be the input of the PID controller in the forward dynamic process of simulation.

The output of the PID controller (G^l) will be transferred to the control muscle actuator in the simulation in parameter ($u_(t)$) in Eq. 9. The G^l is calculated as follows:

$$G^l(t) = G^l_p(t) + G^l_i(t) + G^l_d(t) \tag{11}$$

where the value of $G^l_p(t)$, $G^l_i(t)$, and $G^l_d(t)$, are calculated in Eqs. (12),(13),and (14), respectively.

$$G^l_P(t) = K_p l^e(t) \tag{12}$$

$$G^l_I(t) = K_i \int_0^t l^e(\tau)d\tau \tag{13}$$

$$G^l_D(t) = K_d \frac{dl^e(t)}{dt} \tag{14}$$

The error or tendon length l^e is calculated from the difference between target muscle tendon length l_T and current tendon length ($l_{mt}(t)$). Parameters K_p, K_d, and K_i are the constant gain parameters for proportional, derivative and integrator. The target muscle tendon length l_T comes from the human kinematic data. Based on the preliminary experiment shown in the supplementary material Section V-B, we set K_p, K_d, and K_i as 50, 100, and 0.01, respectively.

To integrate environmental factors, we integrated the proposed model with real-time external sensory information with a sampling rate of 30 Hz. There are external force sensors F^D(t) from the door sensor, where D_c is the door condition, F^{H_x} is the door handling force in the x-direction (N), F^{H_y} is the door handling force in the y-direction (N), and F^p is the door handling position in the z-direction (N). These information provided by these sensors will be the input of artificial force by the hand of the human musculoskeletal model. Furthermore, mat sensor information $F^{M_1}, \ldots, F^{M_{10}}$ (N) is provided to give the input of the normal force of both

legs while opening the door. The sensory feedback will be calculated internally in forward dynamic of simulation as follows

$$\dot{v} = M^{-1}(\tau + J^T - c) \tag{15}$$

where, $\dot{v}$ is the value of joint acceleration given per unit of time, $M(q)$ is the inertial joint space, $J(q)$ is the constraint Jacobian, f is the constraint force, and c is the bias force (such as Coriolis, centrifugal, or gravitational).

To generate the external force, we applied three-dimensional force and torque to the hand in the human musculoskeletal model. We used the function "**mj_applyFT**" to calculate the applied forces (τ) in every degree of freedom from the given force and torque to the hand. The applied forces (τ) are stored in the variable "**qfrc_applied**" in the MuJoCo systems. These values depend on the external force input.

IV. ENVIRONMENT OF LIVING LAB

A "living lab" is a room containing many integrated sensors for a seamless monitoring system. The proposed living lab is similar to a Japanese single room. It contains a bed, mattress, cupboard, and kitchen. The toilet is not included in the current living lab. The layout can be seen in Fig. 4. There are several sensors included in the room, which are: Two Kinect Azure sensors for human pose recognition, two webcam cameras for human activity detection, one webcam camera for object detection, one pair of pressure sensor installed in the pair of sandals, vibration sensors in the bed, ten pressure sensors in the mat, six loadcell sensors in door handles, and one leap motion sensor for hand pose recognition. We used body tracking developed by Microsoft for Kinect Azure [46]. The Kinect camera recognition can identify the coordinates of the points which belong to a specific person and output their positions in 3D. This paper focuses on the handle sensors and door sensor.

We attached force sensors to common tools to monitor force exerted in natural daily use. We expect that the subject will not feel themself being monitored. Two sensors are discussed in this paper, the handle sensor and the door sensor. The handle sensor may analyze the gripping force and lifting force during the action of transitioning from sitting to standing. The door sensor will; provide data to analyze the subject's strength when opening the door. The door will remain open for several seconds to analyze the muscle's isometric strength during the opening process.

V. EXPERIMENTAL RESULTS

To validate the effectiveness of the proposed model, We conduct some preliminary experiments to validate the kinematics, control systems, and the dynamics systems, explained in Section V-A, V-B, V-C. Then we conduct validation experiments, and application experiments on muscle monitoring while interacting with environments, in Section V-D and V-E.

A. ANALYSIS OF MOMENT ARM

To validate the kinematic of the simulation of the skeleton model, we calculated the moment arm by moving shoulder and elbow joints. Then, we analyzed the moment arm of the Deltoid Anterior, Medial, and Posterior muscles to the three joint angles of shoulder joints (Shoulder flexor/extensor, shoulder elevation, shoulder rotation). We compared the proposed model with several other models. We divided the moment arm analysis into four parts: 1) Single joint positions of moment arm in shoulder and elbow joint 2) Shoulder abduction joints moment arm 3) Shoulder rotation joints moment arm 4) Elbow joints moment arm

1) SINGLE JOINT POSITIONS OF MOMENT ARM IN SHOULDER AND ELBOW JOINT

To validate the proposed model, we compared the moment arm with experimental data provided in [10]. In Figure 5, the muscle moments were compared with study of Holzbaur et al. [10], Otis et al. [47], Liu et al. [48], Hughes et al. [49], and Kuechle et al. [50]. The data from the proposed model are shown in red diamond marker. The rotation and abduction moment arm in Subscapularis (SUBSC), Supraspinatus (SUPRA), Infraspinatus (INFRA), and Teres minor (TMIN) are located near the reference experimental data. In Figure 5(b), the moment arm of Deltoid anterior (DELT1), Deltoid Medial (DELT2), and Deltoid posterior (DELT3) are analyzed from the flexion-extension and adduction-abduction viewpoints. We compared our study with the experimental studies of Holzbaur et al. [10], Otis et al. [47], Liu et al. [48], and Kuechle et al. [50]. There is a big range in the moment arm, especially in the Deltoid posterior muscle (DELT3). However, the proposed model is still within the acceptable range of the experimental data references, and the flexion and abduction joints are also within the acceptable ranges. In Figure 5(c), the moment arm of the references also have big ranges between Holzbaur et al. [10] and Kuechle et al. [50]. The proposed model has similar moment arm to the Holzbaur model. In the elbow joint comparison shown in Figure 5(d), the proposed model also has similar moment arm data to that of Holzbaur et al. [10] and Murray et al. [51].

2) SHOULDER ABDUCTION JOINTS MOMENT ARM

We compared the moment arm of shoulder joints with moment arm data provided in [52]. Figure 6 shows the comparison of shoulder elevation (abduction moment arm) Supraspinatus (A), Infraspinatus (B), Teres Minor (C), Subscapularis (D) and Deltoid (E) over a range of shoulder abduction angles. We moved the shoulder elevation and abduction from 0 DEG to 90 DEG, with other joints (Shoulder Rotation, Flexion, and Elbow joint) remaining at 0 DEG. As a result, all of the proposed muscles have similar direction.

The supraspinatus muscle has a similar moment-arm value at 0 DEG, and has a difference of around 2 cm at 90 DEG. However, this muscle has a similar direction. The proposed

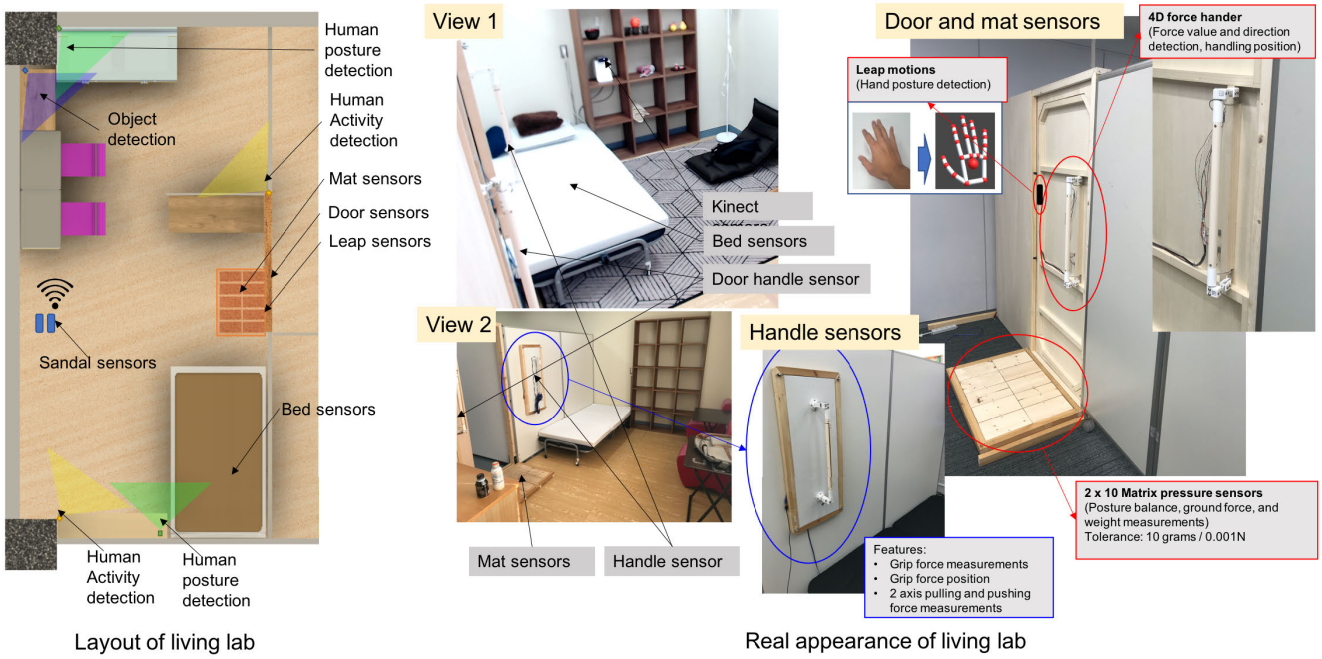

FIGURE 4. Layout of living lab that is used in the proposed experiments.

infraspinatus moment arm is still in the range of fiber muscle of Webb et al. [52]. In the teres minor muscle, the moment arm from the proposed model is negative, which is similar to the comparison models. The moment arm in the Subscapularis muscle, has a similar value across the range of the joint, with only 3 mm of difference. In the deltoid muscle, the proposed model has similar characteristics to the Holzbaur model. The Deltoid medial muscle has similar moment direction across the joint range. At 0 degrees, all the models of the in Deltoid anterior muscle have similar values with a positive direction. In the 65 DEG, the proposed model of moment arm changes to negative direction, while the Holzbaur model changes the moment direction at 50 DEG. Furthermore, the moment arm of the proposed model has similar value with Holzbaur model at 90 DEG. Then, it has 1 cm difference at 0 DEG of shoulder abduction angle.

3) SHOULDER ROTATION JOINTS MOMENT ARM

We compare the moment arm of the shoulder joint with moment-arm data provided in [52], as shown in Figure 7. We show the comparison of shoulder rotation of Supraspinatus (A), Infraspinatus (B), Teres Minor (C), Subscapularis (D) and Deltoid (E) over a range of -45 DEG to 45 DEG of shoulder rotation, with Shoulder Elevation, Flexion, and Elbow joint remaining at 0 DEG.

The proposed model has a moment arm of Supraspinatus, Infraspinatus, and Teres minor muscle with similar characteristics to the Holtzbaur et al. [10] model (see Figure 7 A, B, C). It is within the range proposed by Webb et al. [52]. In the Subscapularis muscle, the proposed model has a similar moment arm to the Holzbaur model in 10 DEG of joint angle and has 6 mm of difference at 45 DEG. It has in the range of the Webb model. All the models have similar moment directions In the deltoid muscle shown in Figure E, The moment arm of the Deltoid posterior has 4 mm of difference compared to the Holzbaur model, and it has similar direction. In the proposed Deltoid medial, there is a big difference of the moment arm from the Holzbaur model in the internal rotation, but the moment arm value is in the range of the Webb model. The proposed model of the Deltoid anterior muscle has similar characteristics to the Holzbaur model, including the same moment direction and moment value of 0 in -35 DEG of rotation joint.

4) ELBOW JOINTS MOMENT ARM

In the elbow flexor analysis, we move the elbow joint from the straight position 0 DEG to maximum flexed position (130 DEG). The forearm joint angle was set in the neutral forearm position (Zero Deg, or mid- pronation/supination). We compared ten upper-extremity specimens from the study of Murray et al. [51]. As a result in Figure 8, the proposed Brachioradialis, Biceps, ECRL, Bracialis, Triceps, and Pronator teres are in the range of the moment arm distribution from 10 specimens. Brachioradialis muscle has 0 moment arm in a straight configuration and 8 cm in 90 degrees of flexor. The Bicep muscle has 7 mm of moment arm in a straight configuration and 45 mm in 90 deg of elbow flexor. ECRL muscle has 0 moment arm in 16 degrees and 29 mm in 90 deg of elbow flexor. Brachialis muscle has 0 moment arm in 9 degree and 23 mm in 90 deg of elbow flexor. The triceps muscle has negative joint moment, where

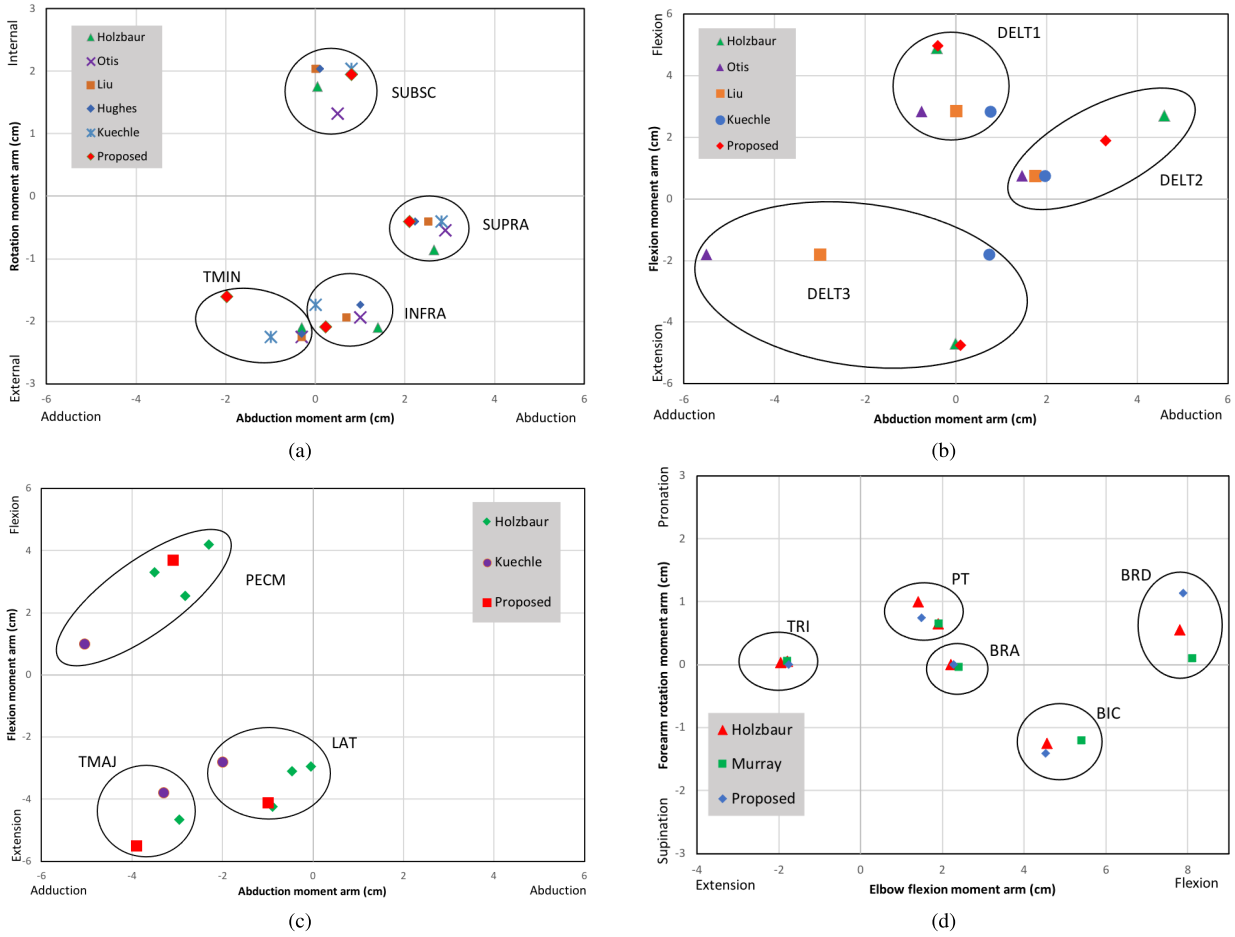

FIGURE 5. Comparison of the moment arm at the upper limb a) the rotator cuff of shoulder b) the three segments of deltoid muscles c) the other muscles including Pectoralis major (PECM), Latissimus dorsi (LAT), and Teres major (TMAJ) d) the muscle in elbow joints. In a), the shoulder rotation and abduction moment arm are calculated with 60^o of shoulder abduction joint and 0^o of rotation joint. In b) and c) the shouder flexion and abduction moment arm were calculated in neutral position with elbow flexion in 90^o.

in 0 DEG, it has -20 mm of moment arm and -16 mm in 90 deg of elbow flexor. Pronator Teres muscle has positive joint moment, in 0 DEG it has 2 mm of moment arm and 15 mm in 90 deg of elbow flexor.

In the forearm rotation analysis, we rotated the forearm joint angle from −90 (maximum pronation) to 90 (maximum supination) with elbow flexed to 85 DEG. We compared the male and female model specimens from the study of Murray and the fresh cadaver specimen from the studies of Bremer, and Saul's OpenSim model. In the pronator teres moment arm, the proposed model has an amplitude similar to the Murray and Bremer studies. The Saul model has a larger magnitude of moment arm. However, all the models have positive joint moment. In the Biceps muscle, the proposed model has a similar value of moment arm to the Saul model. In all muscles the values of moment arm have negative moment arm with range from −10 mm to −16 mm. Furthermore, the Brachioradialis muscle in all the models showed similar characteristics in their moment arm. They have positive moment arms in a supinated position and negative moment arms in a pronated position.

B. EXPERIMENTS OF RESPONSE MUSCLE CONTROL MODEL

To validate the agreement between the target joint angle and the result in simulation, we analyzed the response of the output of the joint angle generated from the muscle forces. We showed the result of different gain parameters in Figure 9. It requires around 100 ms to achieve the stable target position. In this test, we performed the elbow lift and moved the elbow flexor joint from 0 to 90 degrees. A higher value of K_p causes a faster response, but it also caused an overshoot.

To show the effect of the constant parameter on the slow or fast target movement, we conducted experiments as shown in Figure. We analyzed the movement of the elbow flexion joint from the muscle driven. We gave the target movement to the elbow joint from 0 degrees and from the straight position to 90 degrees at three different speeds, 10 rad/s, 2.5 rad/s, and 1 rad/s. We perform the movement for each target speed with five different sets of constant gain parameters.

1) $K_p = 10$, $K_d = 100$, $K_i = 0.01$
2) $K_p = 30$, $K_d = 100$, $K_i = 0.01$

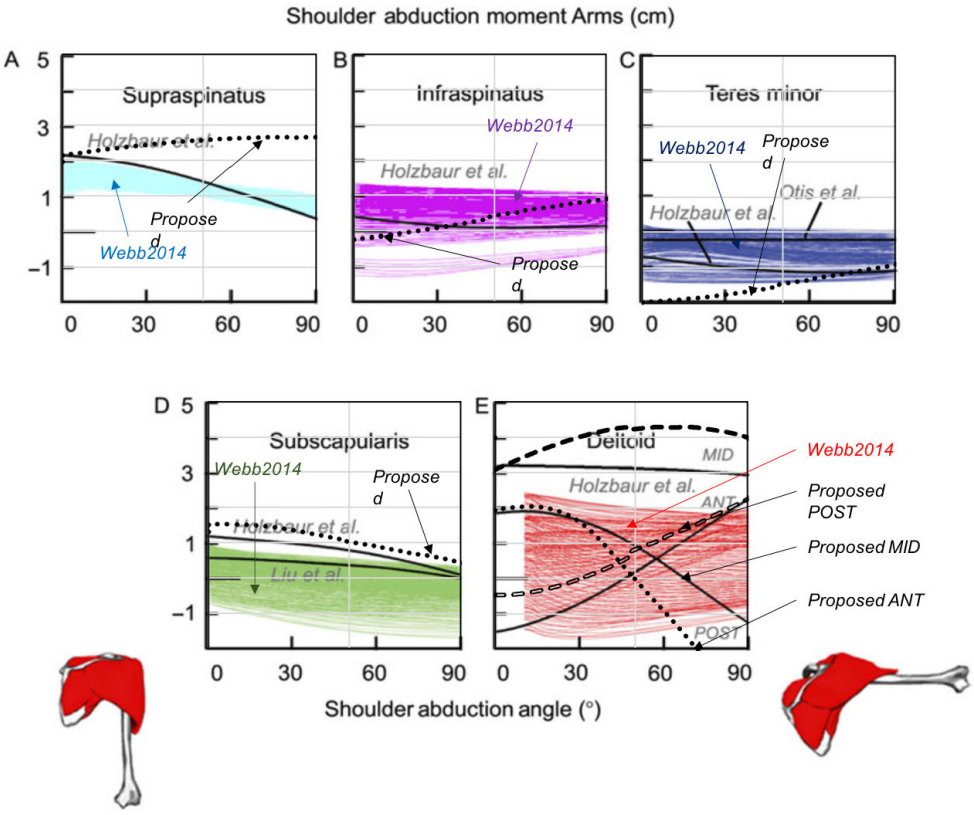

FIGURE 6. The comparison of shoulder elevation joint (Abduction moment Arm) in Supraspinatus (A), Infraspinatus (B), Teres Minor (C), Subscapularis (D) and Deltoid (E) over a range of shoulder abduction angles. The proposed model is compared with finite element muscle model from Webb et al. [52], Muscle model from Holtzbaur et al. [10], and experimental measurements from Liu et al. [48], and Otis et al. [47]. ANT, MID and POST in figure E represent the deltoid anterior, middle, and posterior of Holzbaur model [10].

3) $K_p = 50, K_d = 100, K_i = 0.01$
4) $K_p = 100, K_d = 200, K_i = 0.01$
5) $K_p = 150, K_d = 200, K_i = 0.01$

The results, in Figure 10, show that the lower gain parameter (No. 1 and 2) cannot achieve the target position at slower or higher speeds. The highest gain parameter (No. 5) has overestimation and oscillation in slower and higher joint speed. The gain parameter No. 3 and 4 have less oscillation and is able to achieve the target position at any joint speed. Therefore, the faster movement is not required for the higher gain parameter and slower movement is not required for the lower gain parameter.

In the implementation, test movements were slower than human gait or functional arm movements. This is caused by a delay from the human-skeleton-recognition process and the delay from muscle-driven control. The choice of gain parameter may also cause the delay of movement. Previously, in the validation experiments in Section V-D we just defined the K_p K_d K_i as 50, 100, 0.01. However, it can be optimized to achieve better response.

C. ANALYSIS OF PHYSICS DYNAMICS

In inverse dynamic analysis, velocities and acceleration are computed by differentiating the positions. The inverse dynamic is calculated as follows:

$$\tau = M\dot{v} + c - J^T f \tag{16}$$

where, $\dot{v}$ is value of joint acceleration is given in every time step. $M(q)$ is inertial in joint space $J(q)$ is constraint Jacobian, f is the constraint force, c is bias force such as Coriolis, centrifugal, gravitational. We analyzed the forces, moments, and joint angles during two performances, elbow lift and back curl, with and without holding the 5 kg barbell load.

In the elbow lift performance, shown in Figure 11(a), the *brachialis* and *brachioradialis* muscles sustain significant force during the load. The biceps muscles also increased the force value. In the first 150 ms, there is a high force impact to move the elbow flexion joint from 0 degrees (straight position) to 90 degrees. The torque of the joint has a high value when the elbow moves from 0 degrees to 90 degrees. However, it becomes zero after the elbow joint remains at 90 degrees.

In the back curl performance, shown in Figure 11(b), the *Deltoid Posterior*, *Brachialis*, and *Brachioradialis* muscles have significant force during the load. In the first 200 ms, there is a high force impact to move the elbow flexion and shoulder elevation joint from 0 degrees (straight position) to

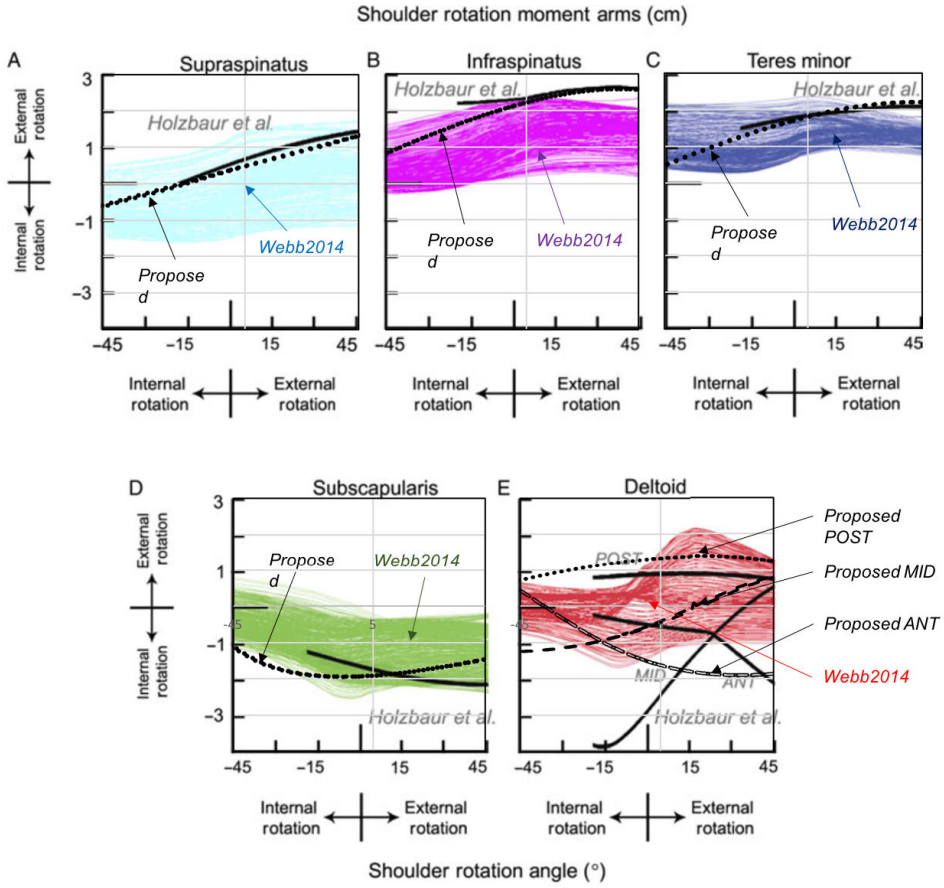

FIGURE 7. The comparison of shoulder rotation joint in Supraspinatus (A), Infraspinatus (B), Teres Minor (C), Subscapularis (D) and Deltoid (E). The proposed model is compared with the finite element muscle model of Webb et al. [52] and the Muscle model of Holtzbaur et al. [10].

90 degrees. The torque of the joint has a high value when the elbow and shoulder move from 0 degrees to 90 degrees. However, it becomes zero after the elbow joint remains at 90 degrees.

Furthermore, we compared the torque output from inverse dynamics and from muscle-driven simulation in the elbow joint. We moved the elbow joint from 0 deg (straight position) to around 90 degree by driving four muscles, BIClong, BICshort, BRA, BRD. We put external forces of 50 N in the gravitational direction from the hand. The result has shown in the Figure 12. The red line represents the total torque from four muscles, the purple line represents the torque from the external load, and the blue line represents the torque from inverse dynamics. The torque from inverse dynamics can generate the same value comparing to the torques from muscle driven with torque from external load. To show the effect of gain parameters to the torque output, we compared between lower gain and higher gain as shown in Figure 13. Graph A represents a lower gain parameter with $K_p = 30$, $K_d = 100$, $K_i = 0.01$, and Graph B represents a higher gain with $K_p = 100$, $K_d = 200$, $K_i = 0.01$. We analyze the gap range between muscle driven torque and inverse dynamics torque. The higher constant gain parameter has bigger gap than the lower gain parameters.

D. VALIDATION EXPERIMENTS

To validate the simulation with regard to muscle activity, we recorded muscle activity using EMG sensors by Delsys Trigno. We compared these results to the muscle activity from the simulation. We attached EMG sensors to the peak contraction area of the muscle. There are ten muscles to be recorded, which implies that ten sensors will be attached. They attachment muscles are: 1) *Brachioradialis*, 2) *Biceps*, 3) *Triceps*, 4) *Deltoid Anterior*, 5) *Deltoid Medial*, 6) *Deltoid Posterior*, 7) *Pectoralis Major*, 8) *Latissimus Dorsi*, 9) *Flexor Digitorum Profundus*, and 10) *Extensor Digitorum Communism*.

Four healthy subjects with variant height (165, 175, 170, and 173 cm), ages 36, 31, 30, and 40,and weights (56, 67, 73, and 80 kg) took part in this experiment. This study has been approved by Ethical, Legal, and Social Issues (ELSI) of Tokyo Metropolitan University, Japan. All participants prepared informed consent prior to this study.

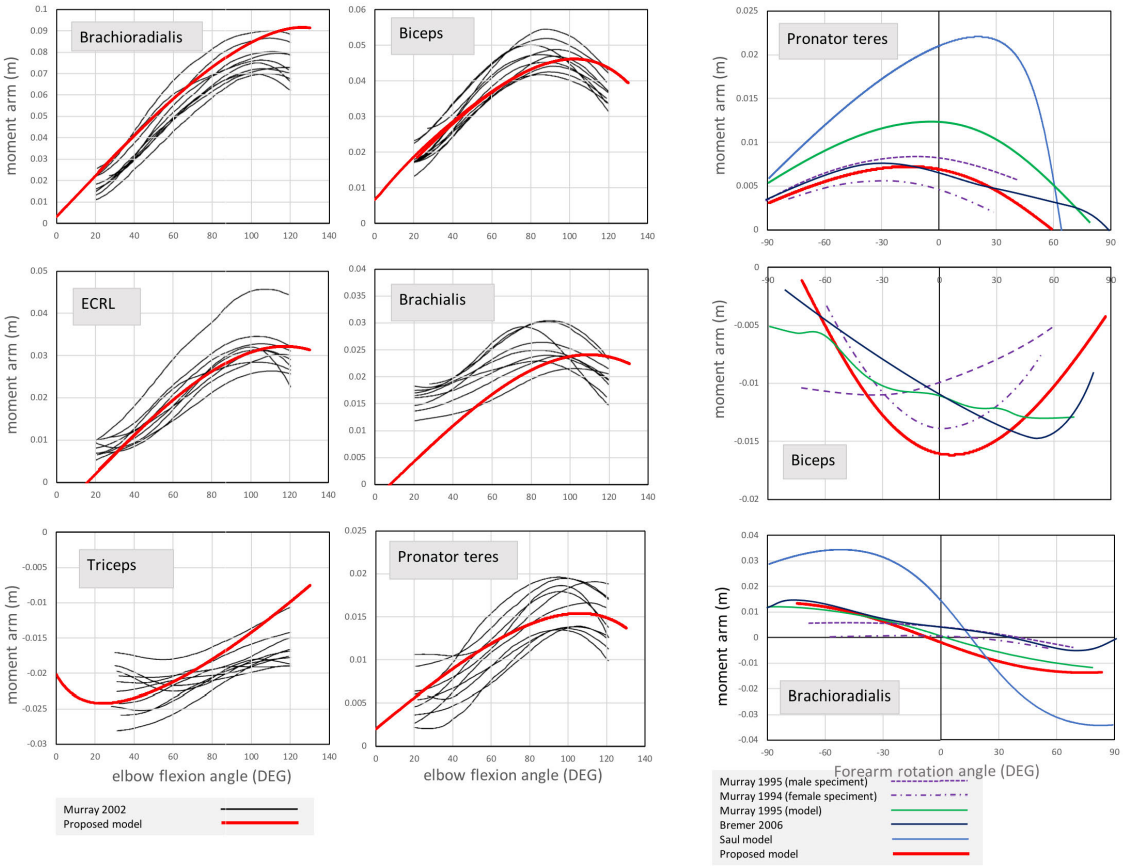

(a)

FIGURE 8. The comparison of moment arm in elbow flexor and forearm rotation joint angle. The moment arm in elbow flexion joint comparison in provided by experimental data of Murray et al. [51]. The moment arm in forearm rotation is compared with several data from Murray et al. [51], study of Bremer et al. [53], and Saul's simulation model in opensim [4].

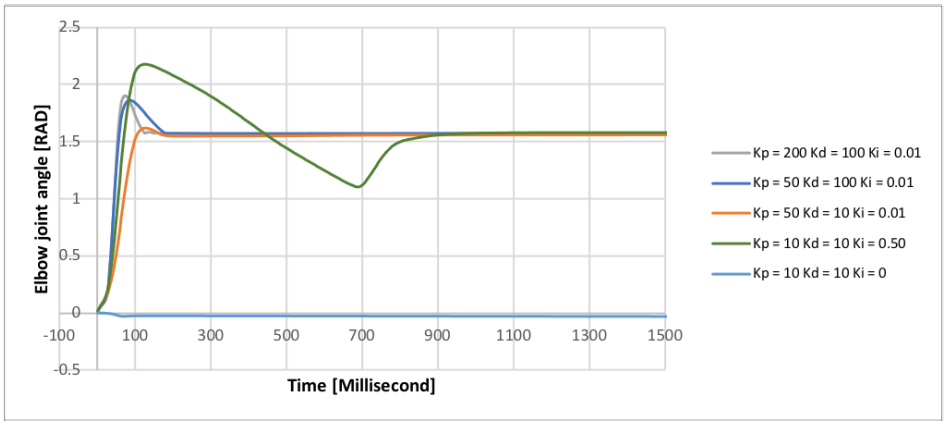

FIGURE 9. Comparison of control response in different constant parameters.

1) DATA ACQUISITION

The subjects were asked to plan a sequence of tasks. The Delsys sensors collected the EMG data for each subject as they performed the actions. We considered the data collection setting based on the study of Ives and Wigglesworth [54], which has established the best sampling rate for acquiring sEMG data. According to this research, under-sampling can result in data loss, and over-sampling (above 1000 Hz) is not required to capture the critical components of the sEMG signal. However, since the memory allocation was not a

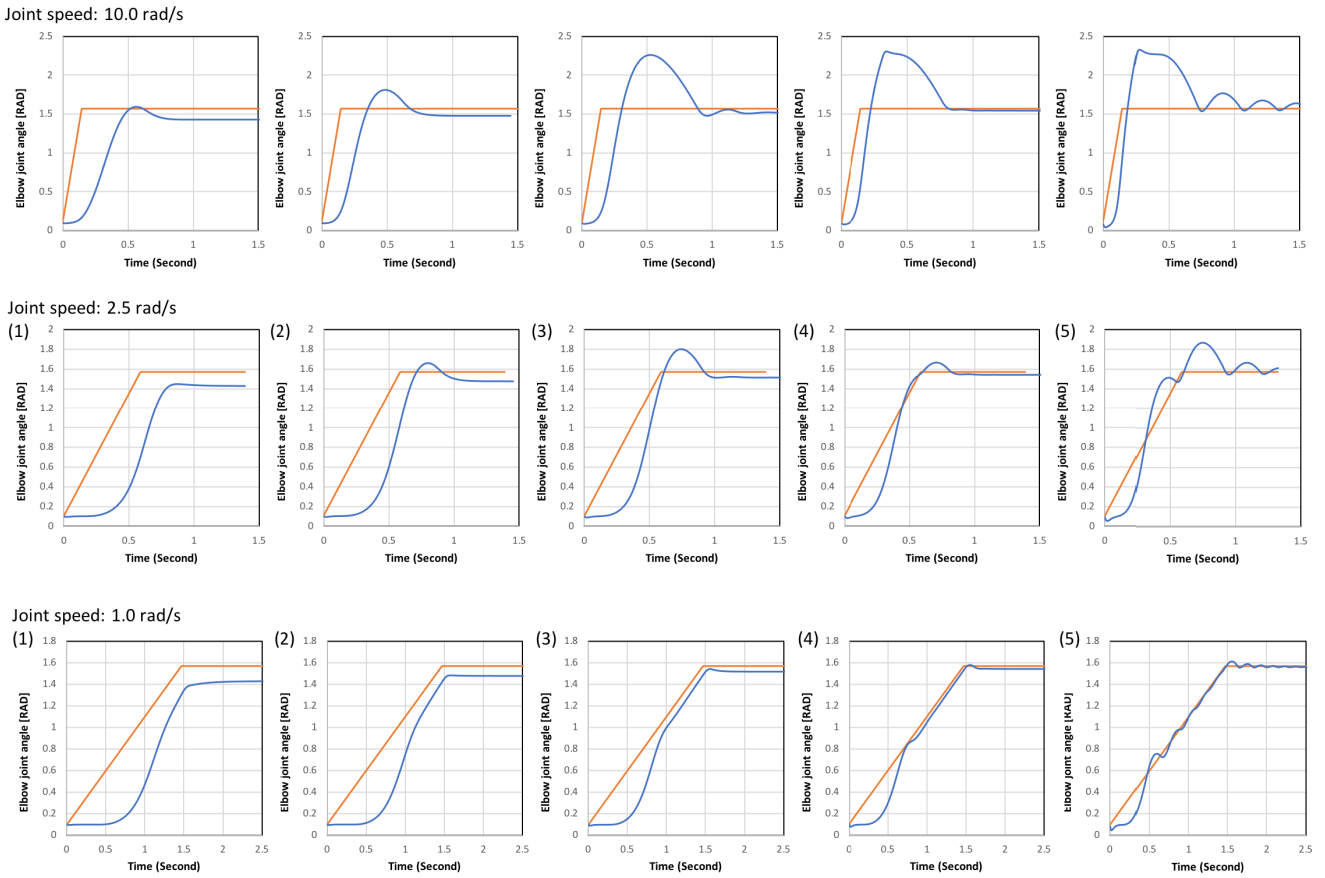

FIGURE 10. Comparison of control response in different constant parameters and target of joint speeds.

problem, we set the frequency to 2000 Hz. The EMG data is recorded together with the proposed real-time musculoskeletal simulation. The experimental documentation can be seen in Supplementary Figure 18 and video experiments can be seen in the Supplementary Video 1 for subject A, Video 2 for subject B, Video 3 for subject C, and Video 4 for subject D.

2) MUSCLE ACTIVITY COMPARISON

In this part, we compare the muscle activity generated by the proposed simulation of our human musculoskeletal model and the EMG sensors. The comparison graph can be seen in Supplementary Figure 18. The comparison graph in the Deltoid Anterior muscle (see Supplementary Figure 19(a)) shows the similarity between the control signal and the normalized EMG signal almost in every desired movement. The comparison graph in the Deltoid Medial muscle (see Supplementary Figure 19(b)) shows the similarity between the control signal and the normalized EMG signal in the first, second, and third desired movements. However in the fourth and fifth movements, which are back lift and shoulder back lift, the similarity between the EMG sensor and the control signal is different. The reason may be the attachment of EMG sensors to the posterior area. The comparison graph in the Deltoid Posterior muscle (see Supplementary Figure 19(c)) shows similarity activation in Subjects A, B, and D. It seems there is overlapping EMG sensors attachment in Subject C. The EMG signal of the Deltoid Anterior and Posterior in Subject C has a similar signal. However, three subjects show correct EMG signal where the Deltoid Posterior activated during back lift and shoulder back lift movements. The Glenohumeral joint has a high risk of muscle activation detection. A small error in skeleton detection may cause the error of muscle activation in the simulation. In the case of Deltoid Medial muscle, it may be caused by the error of the shoulder elevation joint. The value of the shoulder elevation joint generated by skeleton detection is more in the adduction direction than the actual value. The actual shoulder elevation tend to be located towards the adduction direction. Therefore, the EMG sensors detect any activation in Deltoid Medial muscle. In the simulation, the Deltoid muscle was not required to generate the force to lift the shoulder elevation joint.

The graph of the Pectoralis Major muscle (see Supplementary Figure 19(d)) does not show any explicit activity. We could not analyze the similarity in this muscle. Then, the comparison graph of the Biceps muscle shows the similarity between the EMG activation signal and the control signal of human musculoskeletal model. Finally, the comparison graph

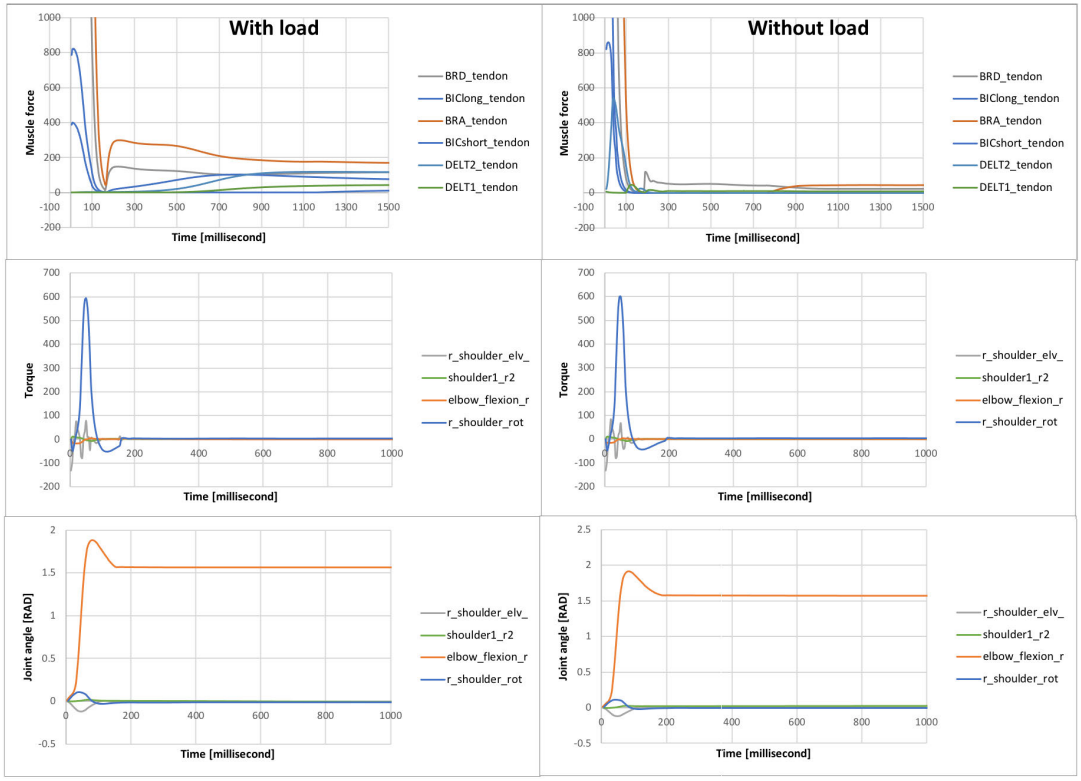

(a)

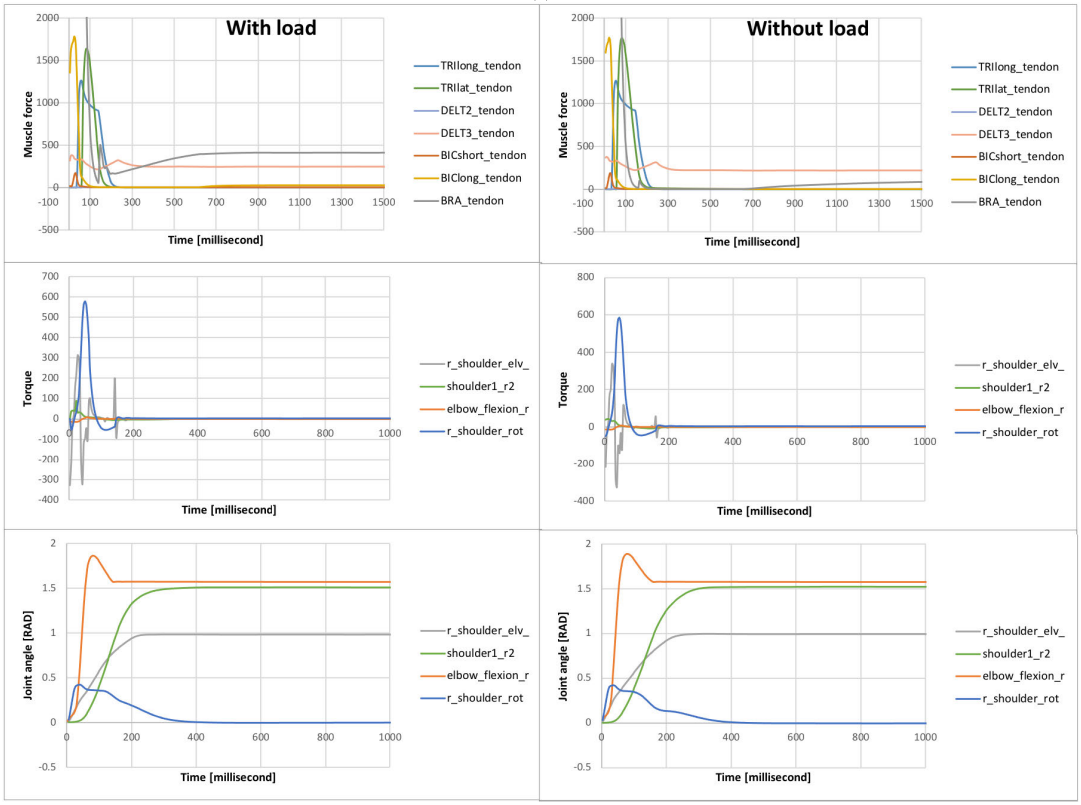

(b)

FIGURE 11. Analysis of dynamic performance a) elbow lift performance b) back curl performance.

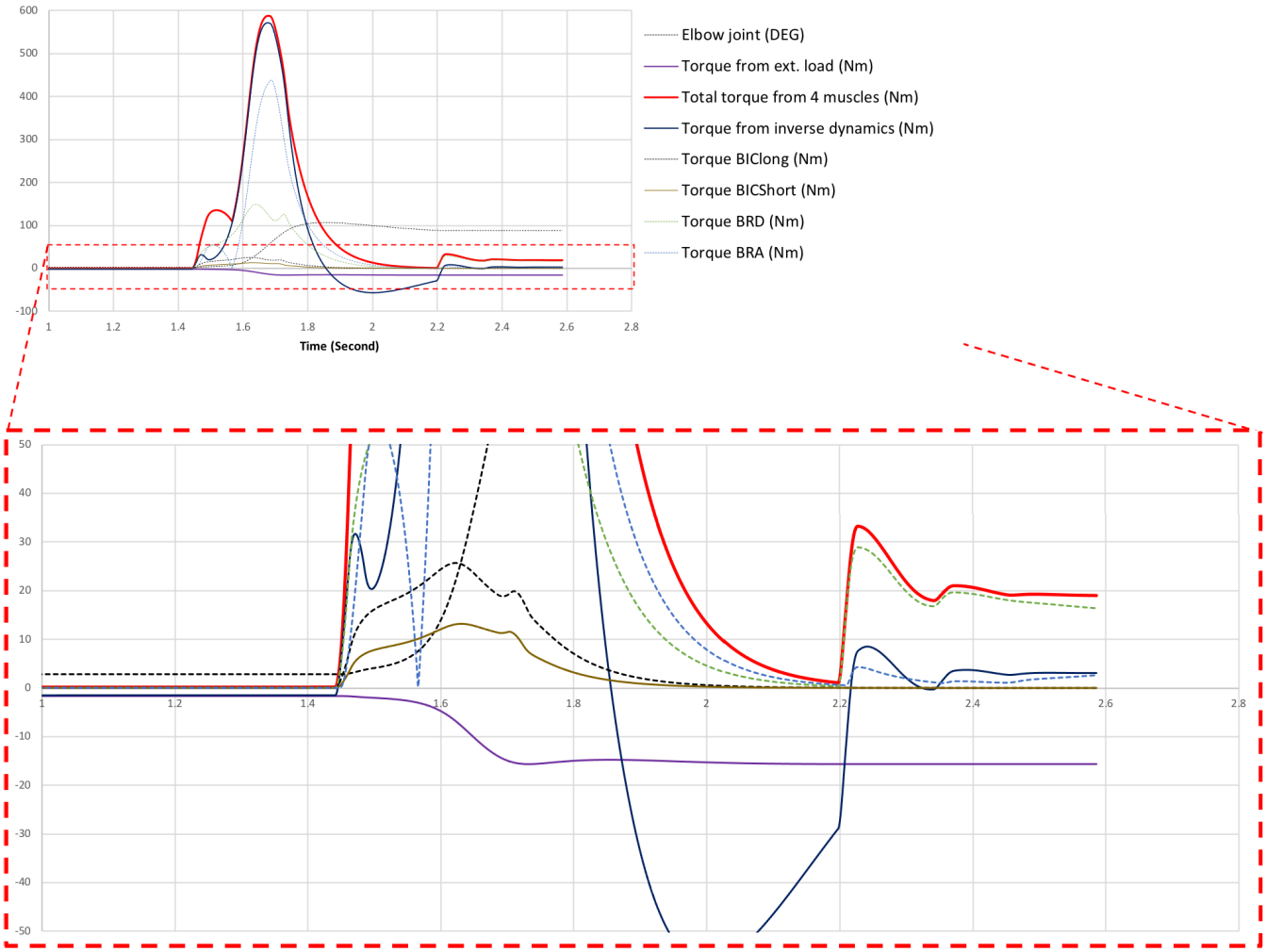

FIGURE 12. The comparison of the torque output from inverse dynamics and from muscle-driven simulation in Elbow joint.

of the Triceps muscle shows the similar activation signal in Subjects A, B, and D. It shows an activation signal during the back lift movement. Furthermore, there is an activation signal of EMG signal in Subject C during shoulder front raise and shoulder side raise movement.

3) MUSCLE FORCE ANALYSIS

Further analysis of muscle force depicted in Supplementary Table 2 shows the force tension generated by each muscle. The force value is acquired from the muscle actuator force generated by MuJoCo. Different scale parameters for each muscle implies that each muscle will have a different maximum force value. Supplementary Table 2 shows the peak muscle force of each subject.

In the maximum force analysis, the ratio of force distribution is similar to the maximum isometric force of actual measurement in [36] and [37]. For instance, in the real measurements of elbow flexor, the maximum force of the Biceps Long Head, Biceps Short Head, Brachialis, and Brachioradialis muscle are 525.1 N, 316.8 N, 1177.4 N, and 276.0 N, which has ratio 1 : 0.603 : 2.24 : 0.525, respectively. In the simulation, the average maximum muscle force has ratio 1 : 0.44 : 1.78 : 0.507. The error ratio of elbow flexed with Bicep long head as muscle reference is 0, 0.266, 0.2, 0.03, and the average error ratio is 0.125. In the real measurement of elbow extensor, the maximum force of in triceps long head, Triceps medial head, and Triceps Lateral head are 771.8 N, 717.5 N, and 717.5 N, which has ratio 1 : 0.929: 0.929, respectively. In the simulation, the average maximum muscle force has ratio 1 : 0.889 : 0.884. The error ratio of elbow extensor with Triceps long head as muscle reference is 0, 0.04, 0.04 and the average error ration is 0.03. Furthermore, in the real measurement of Deltoid muscle, the maximum forces of the Deltiod Anterior, Deltoid Medial, and Deltoid Posterior muscles are 1218.9 N, 1103.5 N, 201.6 N, which have ratio 1 : 0.905 : 0.165, respectively. In the proposed simulation, the average maximum muscle force has ratio 1 : 0.892 : 0.255. The error ratio of Deltoid muscle with Deltoid Anterior as muscle reference is 0, 0.013, 0.368 and the average error ratio is 0.127. The relatively small value

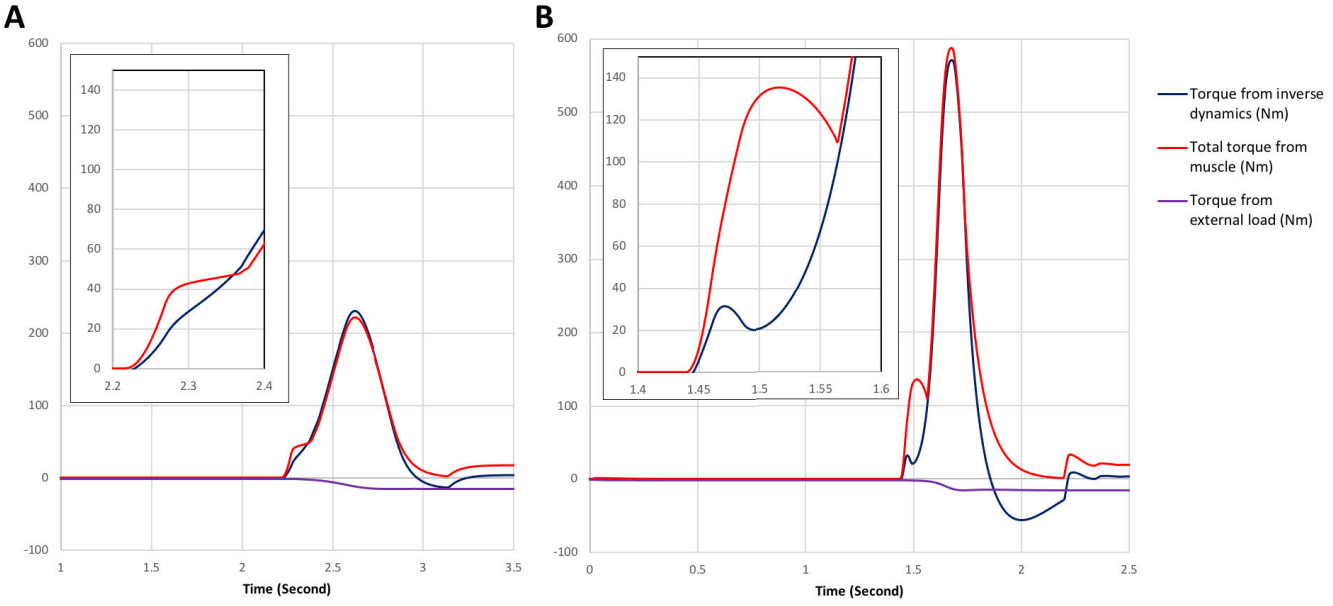

FIGURE 13. The comparison of the torque output between lower and higher constant gain parameters. Graph A represents a lower gain parameter with $K_p = 30$, $K_d = 100$, $K_i = 0.01$, and Graph B represents a higher gain with $K_p = 100$, $K_d = 200$, $K_i = 0.01$.

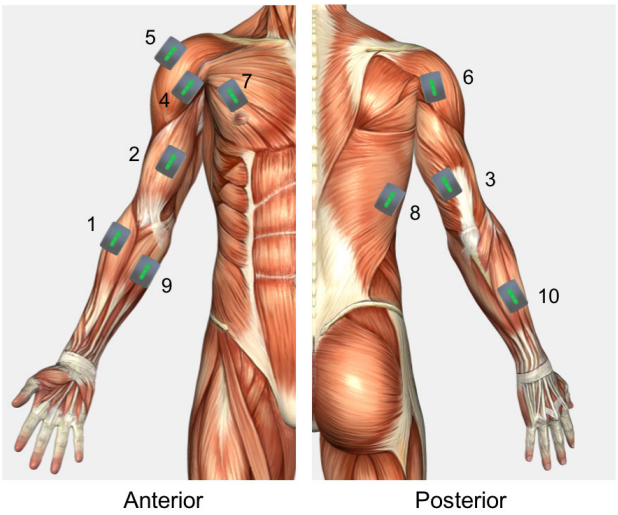

FIGURE 14. Attachment position of EMG sensors. The Delsys sensor placed along the longitudinal midline of the muscles with the arrow parallel to the muscle fibers.

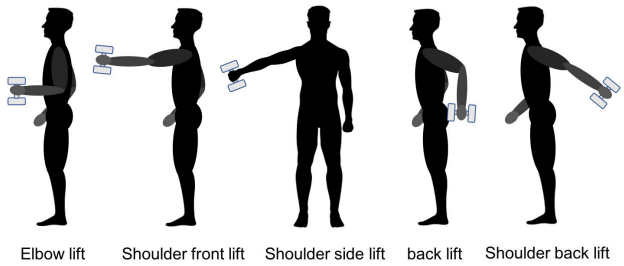

FIGURE 15. Sequence action for experiment validation.

of ratio error implies the proposed human musculoskeletal simulation generates a similar force to the real measurements.

4) QUANTITATIVE ANALYSIS

To improve the validation experiments, we conducted quantitative analysis with different subjects. Five healthy subjects with variant heights (164, 171, 168, 169, and 170 cm), ages 30, 31, 24, 40, and 47 years old, and weights (63, 75, 76, 60, and 78 kg) joined in this experiment. We performed the basic poses of the upper limbs shown in Figure 15 (elbow lift (hammer curl), shoulder front raise, shoulder side raise, back lift, shoulder back lift(triceps kickback)) with grasping a 5kg barbell). This weight will be added as constant external force in the simulation model. Each subject conducted five sets of sequential actions. In one set movement, the user will perform for 15 seconds continuously: three seconds each for the elbow lift, shoulder front raise, shoulder side raise, back lift, and shoulder back lift.

Next, we compared the muscle activity generated from the proposed model with the real muscle activation from the EMG sensors. We analyzed the time on and time off and calculated the error for each set of values. The success rates are calculated as the mean squared error–the average squared difference between the ground-truth values and the EMG sensor values. We calculate the success rate of muscle activation for each action shown in Eq. (17). The error calculation is started from starting time t_{ON} to t_{OFF}. In this experiment, the starting time and end time are defined from the manual analysis. If the muscle is active in i-th pose

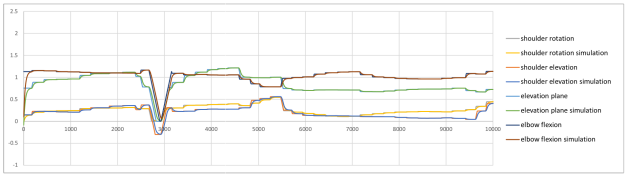

(a)

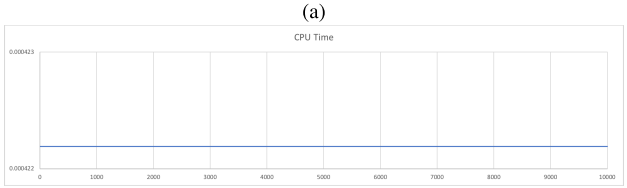

(b)

FIGURE 16. (a) Graph of target joint angle and generated joint angle by human musculoskeletal simulation (b) Graph of CPU time cost.

action, then the value of $u^i_{data} = 1$, otherwise $u^i_{data} = 0$. The ground-truth muscle activation value is acquired from analyzing data from the EMG sensors in the previous validation function. If the ground-truth muscle is active in i-th pose action, then the value $u^i_{REF} = 1$.

$$SuccessRate = 1/5 \sum_{i=1}^{i=5} \frac{1}{t_{OFF} - t_{ON}} \sum_{t=t_{ON}}^{t=t_{OFF}} (1 - (u^i_{REF} - u^i_{REF})^2) \quad (17)$$

Supplementary Video 10 shows the quantitative experiments, which are listed in Table reftable:quant_exp. From their analysis, we achieve a success rate of muscle activation of 0.799, or, nearly 80%. The Deltoid Anterior muscle has better success rate, which is 0.861, followed by the Biceps which achieve 0.854. Triceps muscle activation has the lowest success rate at 0.747. This is because many subjects had difficulties performing shoulder back lift.

5) REAL-TIME ANALYSIS

To analyze the real-time estimation process, we calculate the time difference between each process, from human skeleton recognition to muscle force validation. Figure 16(a) shows the different target joint angles from the simulation's skeleton recognition and joint angle. There is a 100-ms difference between skeletal recognition and human musculoskeletal simulation.

Furthermore, we calculated the time cost for one looping process in computational analysis–shown in the figure 16(b) and the Supplementary Video 9. We calculated this cost as around 0.4 ms. The system can process human musculoskeletal simulations around 2,500 times in one second. However, our computational process only required 1,000 processes in one second.

E. MUSCLE MONITORING WHILE INTERACTING WITH ENVIRONMENTS (LIVING-LAB)

One of the contributions of our proposed musculoskeletal model is its integration with environmental conditions. To show the effectiveness and its applicability, we conducted experiments in the proposed living lab explained in Section IV with several samples of activity, which are 1) analysis of muscle activity while opening doors, and 2) analysis of muscle activity in transitional movement from sleeping to robot-assisted walking (RT-1)

1) ANALYSIS OF MUSCLE ACTIVITY DURING OPENING THE DOOR SENSORS

This experiment analyzed the force and muscle activity measured by the sensors when a person opens the door. The system will ask the person to push or slide the door open with high force and within ten seconds. This proposed model calculates the isometric force while opening the door. This phase only involved one subject. The subject was standing in the living lab, walking to the door, and opening sliding the door using the right hand. The video experiments can be seen in the Supplementary Video 5. The snapshot of video experiments can be seen in Supplementary Figure 20. The graph of muscle control activity can be seen in Supplementary Figure 21.

While monitoring the opening of the door, we could record the activation of Muscle in real-time. There is a significant change of muscle activity or control signal in Deltoid Anterior, Deltorid posterior, Pectoralis Major, Biceps, Teres minor, Coracobrachialis. Deltoid Anterior and Coracobrachialis muscles are activated during opening the door, while Pectoralis major and Biceps muscle have increased of activity. In comparison, the Deltoid posterior and teres minor muscles are deactivated.

2) ANALYSIS OF MUSCLE ACTIVITY IN TRANSITIONAL MOVEMENT FROM SLEEPING TO ROBOT ASSIST WALKING (RT-1)

In this experiment, we analyzed the force and muscle activity when a person moves from a sitting position to a standing position by using RT-1 [55]. RT-1 is the robot that assists with walking for elderly people. Several sensors were installed to support the system. In this experiment, the subject performed the transition action three times with different bed heights, 8 cm, 40 cm, and 60 cm. We use the force sensors in the robot's handle to calculate the pulling or pushing of the hand during transitional movement from sitting to standing. The video experiments can be seen in the Supplementary Video 6, Video 7, and Video 8 for the three bed heights, respectively. The snapshot of video experiments can be seen in Fig. 22. The graph of muscle control activity can be seen in Fig. 23. From this generated control activity, we may analyze the effectiveness of muscle usage.

The transition movement begins with the activity of the biceps muscle. After the user's elbow height was higher than the handle of RT1, the Triceps muscle was activated. There is a significant increase in the Biceps and coracobrachialis muscle in the 8-cm bed height, but there is no activity in the Deltoid middle muscle (see red box). While at 40-cm

TABLE 2. Data of muscle peak force in experiment a (validation).

Muscle	Peak muscle force (N)					Normalized	real	error ratio	average
	Sub. A	Sub. B	Sub. C	Sub. D	Average	ratio	ratio		error ratio
DELT1	1505.804	1505.6409	1466.4876	1487.994	1491.481625	1	1	0	
DELT2	1330.2609	1311.3891	1344.0687	1338.2814	1331.000025	0.892401222	0.905	0.013921301	
DELT3	348.0645	302.653	348.654	348.0789	336.8626	0.225857694	0.165	0.368834507	0.12758527
SUPRA	1696.7727	1701.5701	1702.3117	1692.6377	1698.32305				
INFRA	857.0913	753.4485	1117.0482	886.1542	903.43555				
SUBSC	1501.2691	1500.0441	1500.4039	1502.5026	1501.054925				
TMIN	344.9998	600.3169	493.0592	291.0422	432.354525				
TMAJ	265.4736	473.896	541.1116	539.3318	454.95325				
PECM1	588.7091	371.0417	698.9816	308.8187	491.887775				
PECM2	976.445	1015.4448	935.7671	1011.5369	984.79845				
PECM3	851.5529	1002.209	1012.2971	1004.1438	967.5507				
LAT1	229.1453	145.6846	179.2604	212.4755	191.64145				
LAT2	92.6854	116.9586	109.5314	177.924	124.27485				
LAT3	45.2139	80.1189	52.5222	175.7609	88.403975				
CORB	607.6567	528.4969	537.1323	448.3925	530.4196				
TRILong	708.0564	732.2757	825.8922	821.6032	771.956875	1	1	0	
TRILat	628.1688	616.8226	776.9078	724.2453	686.536125	0.889345179	0.929	0.042685491	
TRIMed	624.4529	613.5844	772.9015	720.0998	682.75965	0.884453098	0.929	0.047951455	0.030212315
ANC	2267.8185	1835.4156	2599.6405	2601.2479	2326.030625				
SUP	1790.3856	1788.5995	1797.8205	1790.4163	1791.805475				
BICLong	570.4192	587.8371	551.0899	580.038	572.34605	1	1	0	
BICShort	208.514	238.5174	285.2806	280.208	253.13	0.442267401	0.603	0.266554891	
BRA	1023.3361	1009.7551	1071.9934	983.7364	1022.20525	1.785991622	2.24	0.202682312	
BRD	266.0317	243.524	305.087	346.4691	290.27795	0.507172103	0.525	0.033957898	0.125798775

TABLE 3. Data of success rate of quantitative experiments.

Subject		Error value						Average Error		
		1	2	3	4	5	1A	Error each set	Muscle Error	Total
Deltoid Anterior	Set 1	0.822	0.779	0.786	0.84	0.764	0.811	0.8	0.861	0.799
	Set 2	0.871	0.828	0.919	0.969	0.821	0.79	0.866		
	Set 3	0.907	0.968	0.945	0.922	0.873	0.82	0.906		
	Set 4	0.845	0.773	0.889	0.847	0.831	0.752	0.823		
	Set 5	0.895	0.911	0.94	0.98	0.972	0.752	0.908		
Deltoid Medial	Set 1	0.876	0.946	0.796	0.783	0.714	0.775	0.815	0.755	
	Set 2	0.787	0.771	0.723	0.664	0.725	0.662	0.722		
	Set 3	0.67	0.628	0.724	0.648	0.65	0.666	0.664		
	Set 4	0.837	0.888	0.768	0.711	0.684	0.809	0.783		
	Set 5	0.78	0.862	0.782	0.798	0.811	0.697	0.788		
Deltoid Posterior	Set 1	0.701	0.687	0.686	0.668	0.637	0.621	0.667	0.777	
	Set 2	0.671	0.576	0.626	0.675	0.536	0.659	0.624		
	Set 3	0.807	0.885	0.829	0.862	0.847	0.703	0.822		
	Set 4	0.845	0.774	0.904	0.825	0.948	0.807	0.851		
	Set 5	0.895	0.989	0.937	0.909	0.969	0.83	0.922		
Biceps	Set 1	0.867	0.793	0.901	0.941	0.804	0.763	0.845	0.854	
	Set 2	0.95	0.844	0.973	0.946	0.969	0.898	0.93		
	Set 3	0.87	0.789	0.852	0.834	0.787	0.752	0.814		
	Set 4	0.825	0.857	0.869	0.88	0.909	0.717	0.843		
	Set 5	0.911	0.887	0.824	0.844	0.759	0.806	0.839		
Triceps	Set 1	0.753	0.789	0.691	0.687	0.681	0.679	0.713	0.747	
	Set 2	0.865	0.847	0.776	0.736	0.755	0.857	0.806		
	Set 3	0.76	0.705	0.689	0.652	0.693	0.719	0.703		
	Set 4	0.716	0.749	0.729	0.674	0.661	0.604	0.689		
	Set 5	0.841	0.603	0.9	0.967	0.908	0.726	0.824		

and 60-cm bed heights, there is no significant increase of control activity in Biceps and coracobrachialis muscle, but there is increasing activity in Deltoid middle muscle. In this experiment, there is no significant difference between bed

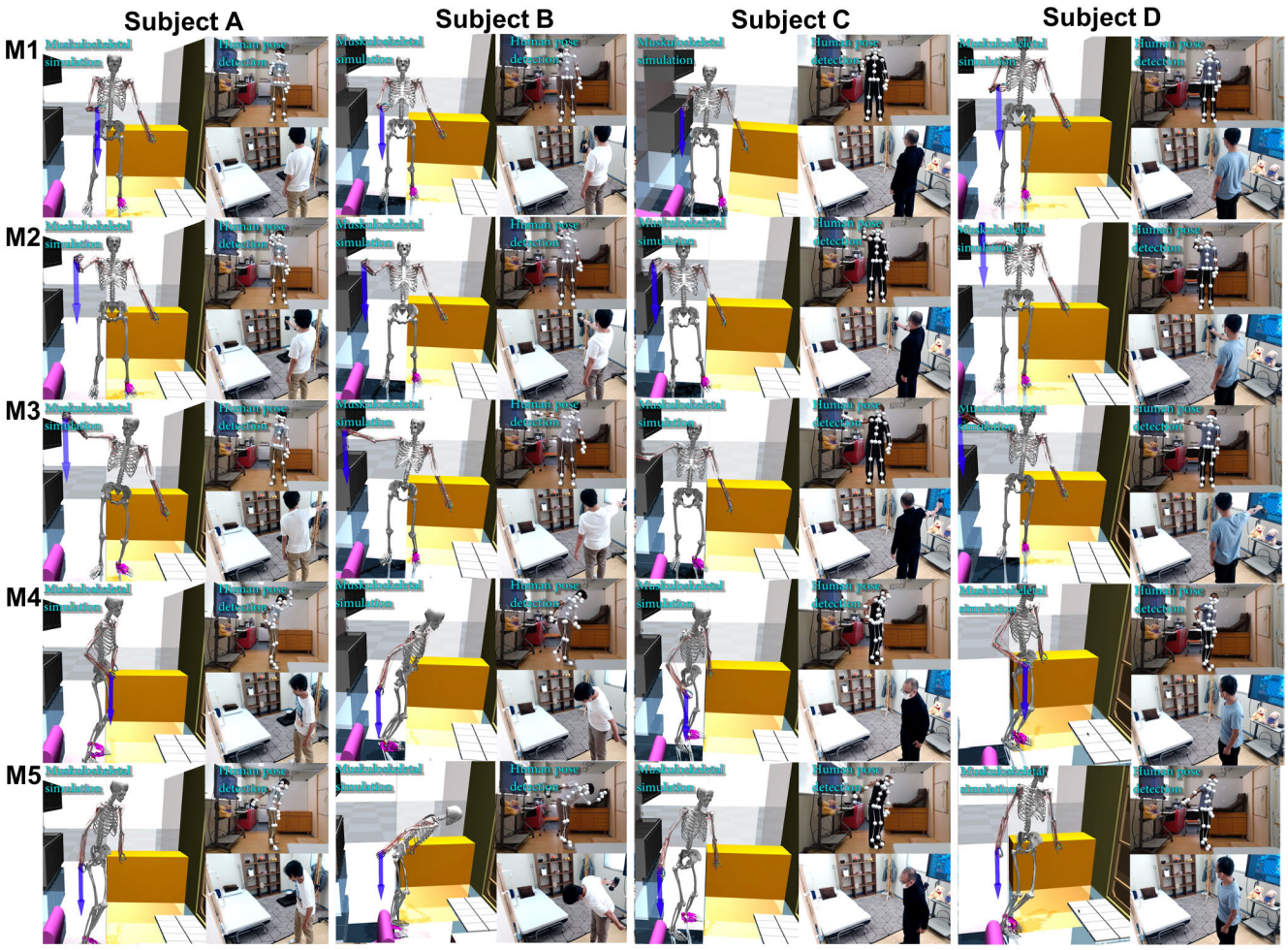

FIGURE 17. Snapshot of validation experiments.

FIGURE 18. Attachment of Delsys EMG sensors in the right hand of subjects.

heights of 40cm and 60cm. From these experiments, we show that the proposed human musculoskeletal model can be successfully integrated with environmental information as the external force feedback.

VI. DISCUSSION AND CONCLUSION

In this paper we have shown how we achieved real-time muscle activity estimation using human musculoskeletal simulation. We focused on the upper extremity of human musculoskeletal model with 50 Hill-type muscles. We built the model in MuJoCo simulation in including surrounding environments as external information to the human musculoskeletal model. The proposed human musculoskeletal simulation can be freely integrated with surrounding environment.

First, we validated the kinematic of the simulation of the skeleton model by comparing the moment arm of muscles related to the three joint angles of shoulder joints (Shoulder flexor/extensor, shoulder elevation, shoulder rotation) and Elbow joints. We compared the proposed model with several

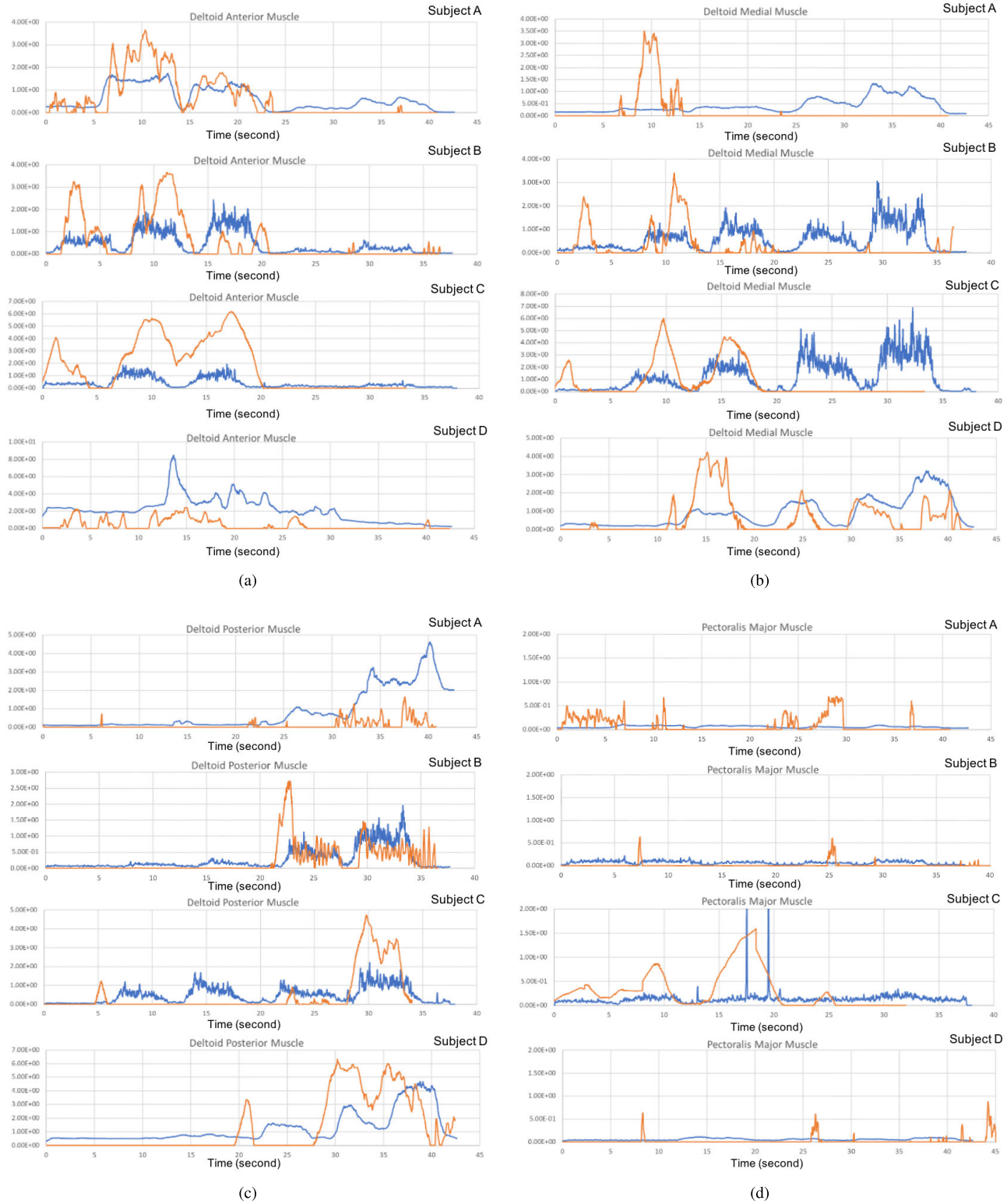

FIGURE 19. Comparison diagram of muscle activity between proposed simulations and real measurement of EMG sensors. There are recorded data from four subjects separated by muscle type. Six muscles are compared in this diagram. (a) Deltoid Anterior muscle (b) Deltoid Medial muscle (c) Deltoid Posterior muscle (d) Pectoralis Major (e) Biceps muscle (f) Triceps muscle. The blue line represents the normalized EMG signal and the orange line represents the control signal in the musculoskeletal model. We use moving window average to filter and normalized data from EMG sensors. We set the window width by considering the quality of the EMG data. In Subject A and D, we set the window width as 750 ms. While in subject B and C which has better EMG data, we set the window width as 75 ms.

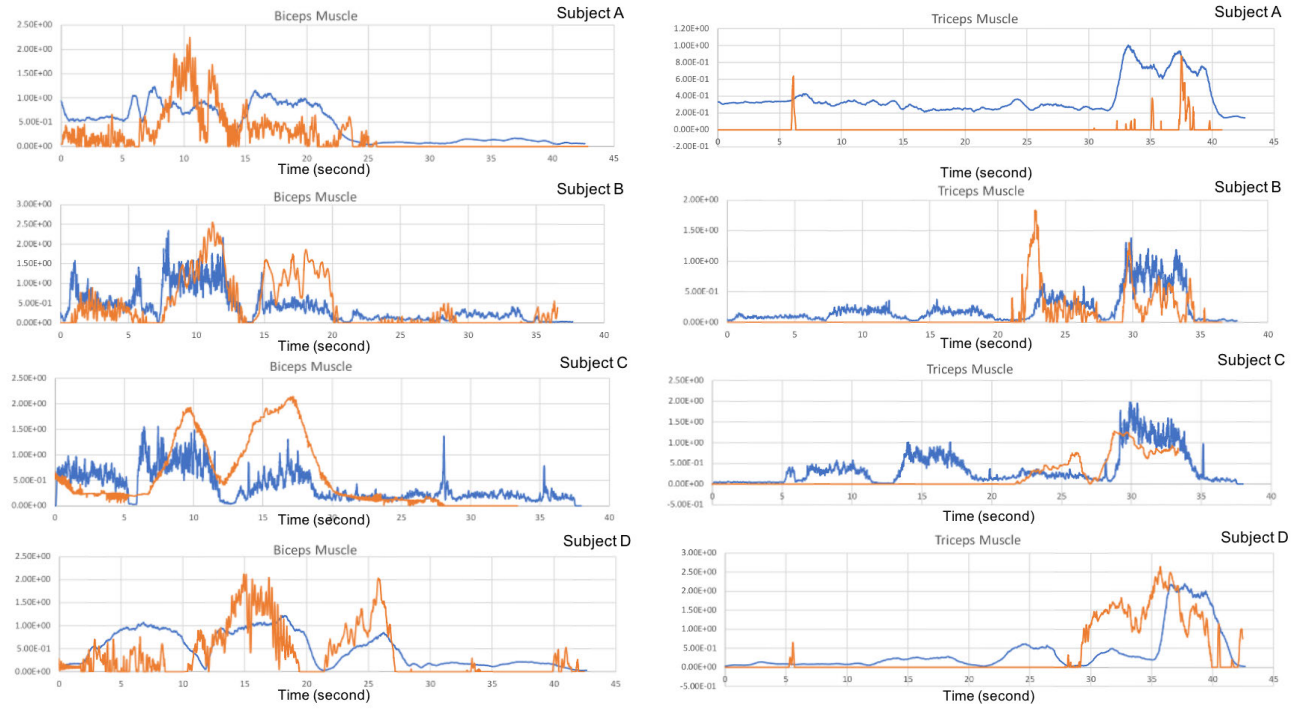

FIGURE 19. ***(Continued.)*** **Comparison diagram of muscle activity between proposed simulations and real measurement of EMG sensors. There are recorded data from four subjects separated by muscle type. Six muscles are compared in this diagram. (a) Deltoid Anterior muscle (b) Deltoid Medial muscle (c) Deltoid Posterior muscle (d) Pectoralis Major (e) Biceps muscle (f) Triceps muscle. The blue line represents the normalized EMG signal and the orange line represents the control signal in the musculoskeletal model. We use moving window average to filter and normalized data from EMG sensors. We set the window width by considering the quality of the EMG data. In Subject A and D, we set the window width as 750 ms. While in subject B and C which has better EMG data, we set the window width as 75 ms.**

other models. As shown in the Supplementary Material Section V-A. The proposed model has similar moment direction in all compared model.

The proposed control model requires gain parameters (K_p K_d K_i) whose settings were acquired from experimental data. We validated the. The result shows that the lower gain parameter cannot achieve target position in slower to higher speed. The higher gain parameter has overestimation and oscillation in slower and higher joint speed. Compromising gain parameter setting is required to achieve less oscillation and able to achieve target position in any joint speed. Delay time response is around 100 ms from the target movement. However, this is still acceptable for the real-time monitoring application which is not required any real action to the user or subject. Decreasing the time response delay will be an aim for the future.

To validate the dynamics model, we compared the torque output from inverse dynamics and from muscle-driven simulation in the elbow joint shown in Supplementary Material Section V-C. The torque from inverse dynamics can generate the same value comparing to the torques from muscle driven with torque from external load. Then, in the effect of gain parameter selection, we compare higher and lower gain parameters setting. The higher constant gain parameter has bigger gap than the lower gain parameters.

To prove the effectiveness of the simulation to the real application, we conducted muscle validation experiments that compare the control activity from the simulation and the recorded EMG sensors. Four subjects were involved in the validation experiments. They performed five planned movements, including: elbow lift (hammer curl), shoulder front raise, shoulder side raise, back lift, shoulder back lift (triceps kickback). We attached 10 EMG sensors which are: 1) Brachioradialis 2) Biceps 3) Triceps 4) Deltoid Anterior 5) Deltoid Medial 6) Deltoid posterior 7) Pectoralis Major 8) Latissimus dross 9) Flexor digitorum profundus 10) Extensor Digitorum Communism. However, we compared 6 muscle (Biceps, Triceps, Deltoid Anterior, Deltoid Medial, Deltoid posterior, and Pectoralis Major) which has significant activity in the desired movement. From the graph shown in Supplementary Figure 18, the control activity has mostly similar with the muscle activity recorded from the EMG sensors. Only one subject in Deltoid Posterior muscle, two subject in Deltoid Medial muscle, and one subject in Triceps muscle which have a different activation. However those errors may occur from the attachment problems.

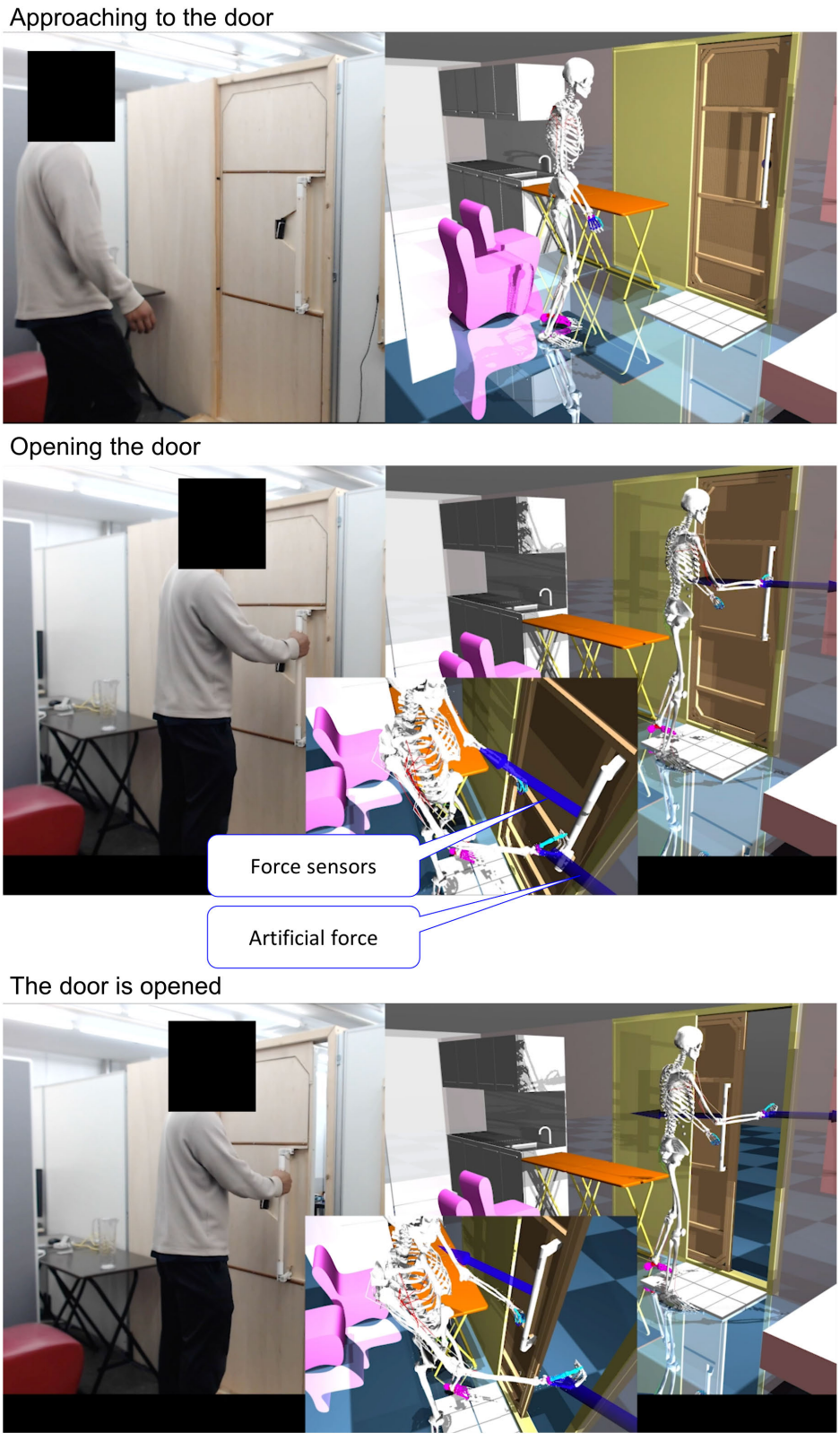

FIGURE 20. Snapshot of experiments during opening sliding door with force sensors.

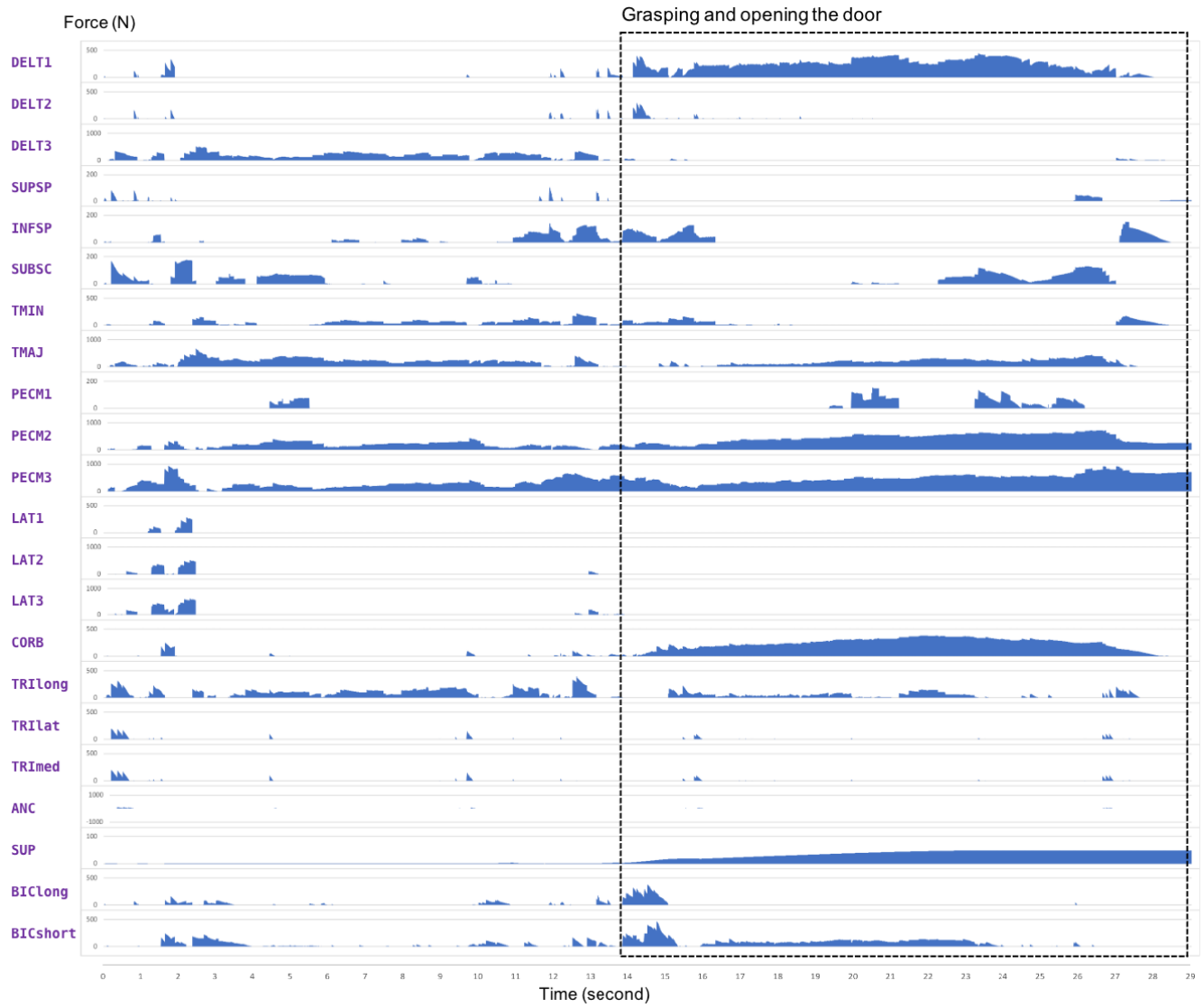

FIGURE 21. Force of muscle graph during opening the door.

Furthermore, we analyzed the maximum force of each muscle in the validation experiment. We compared the maximum force of the Elbow Flexor, the Elbow Extensor, and the Deltoid muscle with the actual measurements of maximum muscle force [36], [37]. We calculate the error ratio of each muscle. As a result, the average error ratio of elbow flexor, elbow extensor, and Deltoid muscle are 0.125, 0.03, and 0.127, respectively. The relatively small error implies that the proposed simulation can generate a similar force value to the actual measurements.

In addition, the experiments show our proposed simulation can be effectively integrated with the surrounding environment and/or artificial environment. We showed two additional experiments that integrated environmental conditions. First, we analyzed the force and muscle activity when a person opened the doors. Second, we analyzed the force and muscle activity when a person moved from a sitting position to a standing position by using RT-1. In the two experiments, we succeeded in measuring and analyzing the muscle activity and muscle force in real-time for further analysis. This method may increase the comfort in human physical monitoring system. The system may recognize the user muscle activity without involving any other person.

Overall, based on the validation by the experiments, the contributions of this paper are as follows:

- Real-time control system of human upper limb muscle activity for human physical monitoring.
- Providing real-time integration between human musculoskeletal model with environmental condition.

In the future work, we will enhance the complexity of the muscle, especially for the hand muscle. We will attach some Leap motion and Hand pose detection from MediaPipe

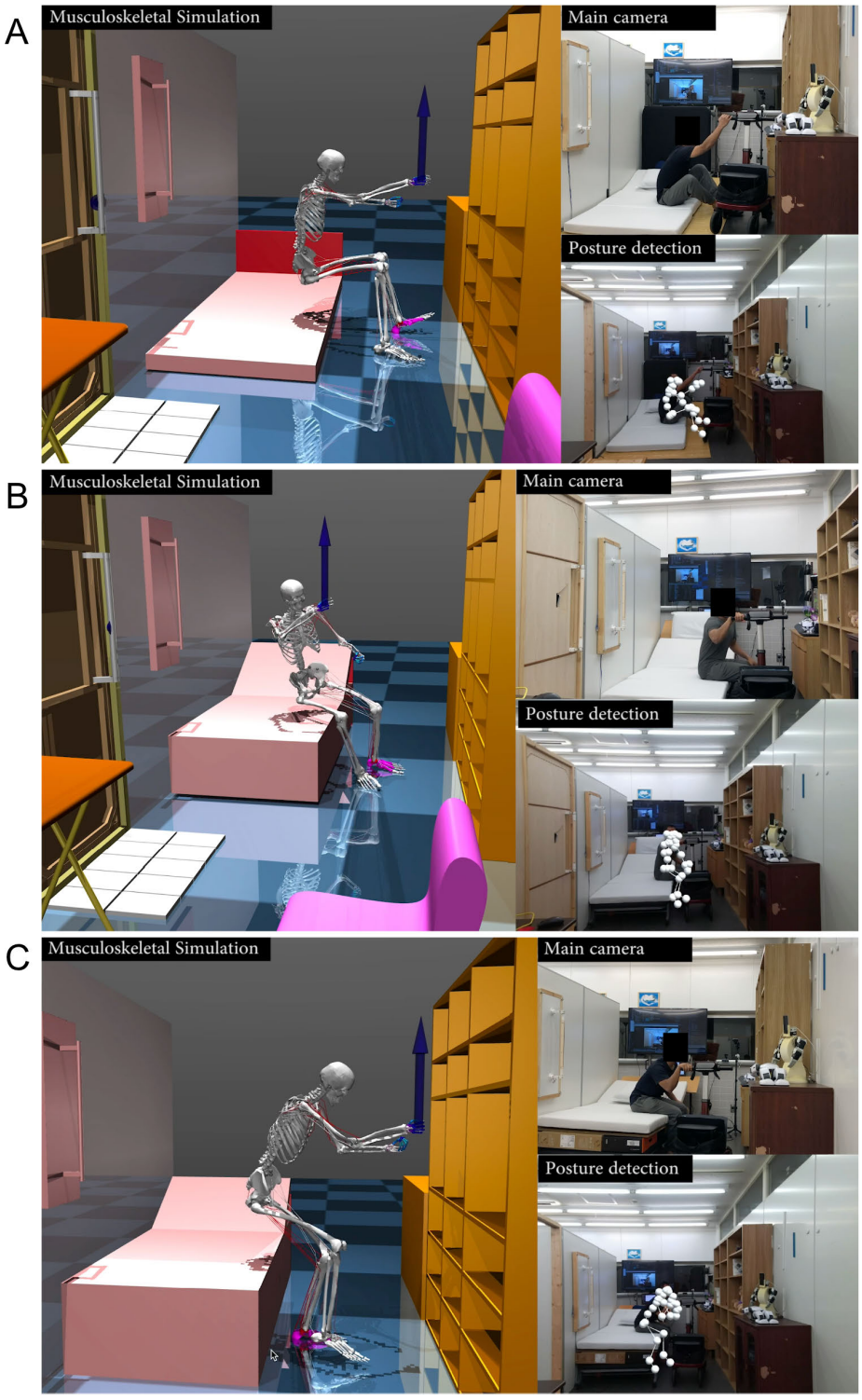

FIGURE 22. Snapshot of experiments using RT1 with different height of bed, A) 8 cm height of bed B) 40 cm height of bed C) 60 cm height of bed.

to recognize the muscle activity of the hand while grasping some tools. Furthermore, we will improve the balance of the human musculoskeletal model by adding some stability control in the proposed system. In addition, the issue of decreasing the time response will be considered as the future works

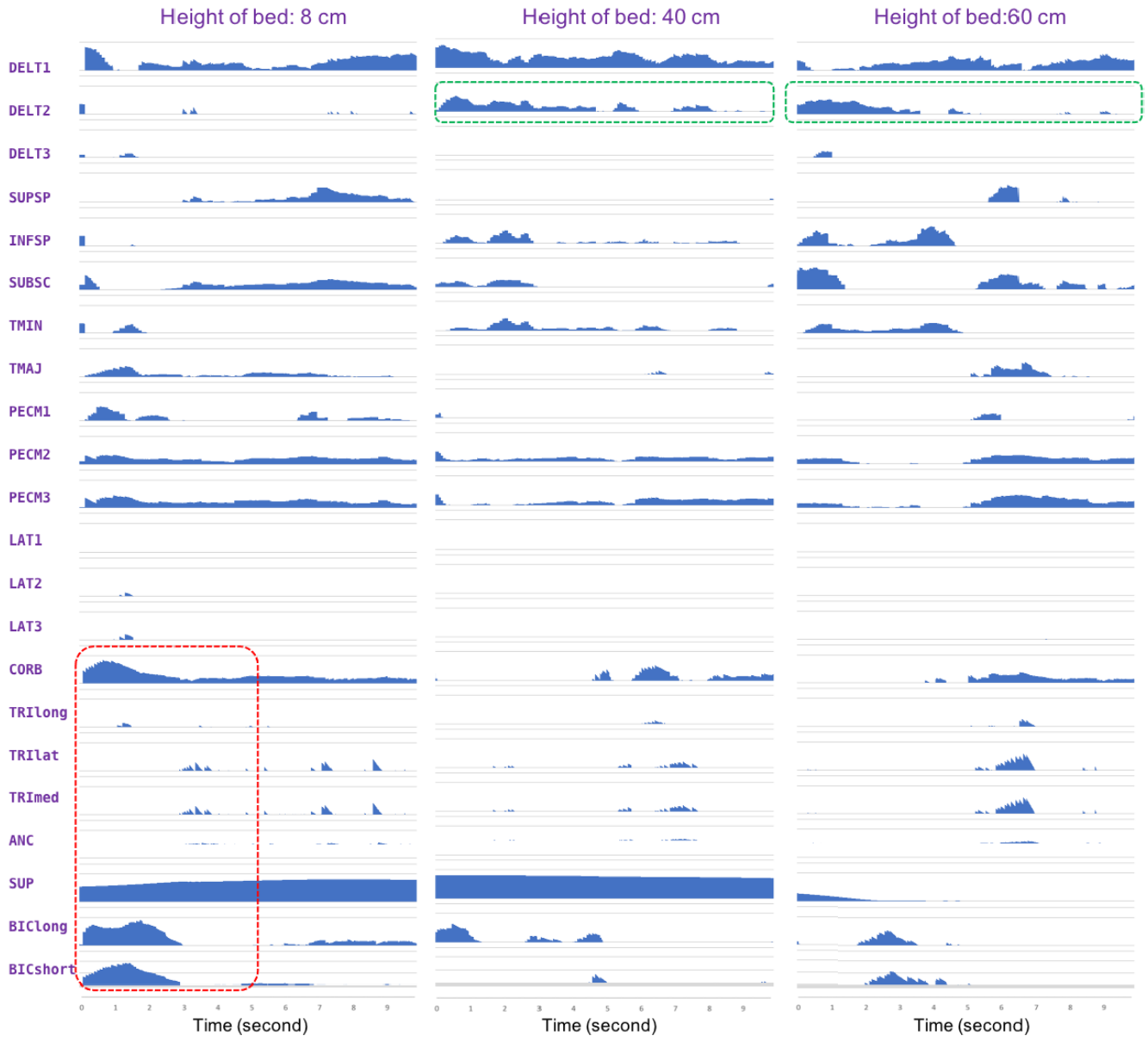

FIGURE 23. Force of muscle graph during transitional movement from sitting to standing using RT1 with different height of bed.

LINK TO THE SUPPLEMENTARY VIDEOS

1) Video of validation experiments of Subject A
   https://www.dropbox.com/s/43vnm2awj63s1mp/data_experiment_right_upper_A.mp4?dl=0
2) Video of validation experiments of Subject B
   https://www.dropbox.com/s/zr8elny70hcg7ih/data_experiment_right_upper_B.mp4?dl=0
3) Video of validation experiments of Subject C
   https://www.dropbox.com/s/fhxtoob54digoe7/data_experiment_right_upper_C.mp4?dl=0
4) Video of validation experiments of Subject D
   https://www.dropbox.com/s/tlegukwpzv5zc1t/data_experiment_right_upper_D.mp4?dl=0
5) Video of experiments during opening sliding door with force sensors
   https://www.dropbox.com/s/mwozljw2vx5tjb6/open%20door.mp4?dl=0
6) Video of experiments using RT1 with 8 cm height of bed
   https://www.dropbox.com/s/esnhc4p1a484efa/WakeUpWithRT1_8cm.mp4?dl=0
7) Video of experiments using RT1 with 40 cm height of bed

https://www.dropbox.com/s/niz4sxf38l59hgf/WakeUpWithRT1_40cm.mp4?dl=0

8) Video of experiments using RT1 with 60 cm height of bed

https://www.dropbox.com/s/e6ln5s3nwxck28f/WakeUpWithRT1_60cm.mp4?dl=0

9) Video of experiments time cost analysis

https://www.dropbox.com/s/6vvv2xw502izafg/time_cost_analysis.mp4?dl=0

10) Video of quantitative analysis of validation experiments

https://www.dropbox.com/s/hw8ggz733bc51gn/Quantitative_experiments.mp4?dl=0

ACKNOWLEDGMENT

The authors would like to thank *Fernando Ardilla, A. R. Anom Besari, and Mohamad Yani* to support the process of data acquisition in validation experiments. They would also like to thank *Dr. Tomoyuki Noda* for their comments and strong discussion. They would also like to thank Kubota Laboratory members to support some developments.

REFERENCES

[1] F. E. Zajac and M. E. Gordon, "Determining muscle's force and action in multi-articular movement," *Exerc. Sport Sci. Rev.*, vol. 17, pp. 187–230, Jan. 1989.

[2] R. Davoodi and G. E. Loeb, "MSMS software for VR simulations of neural prostheses and patient training and rehabilitation," in *Proc. MMVR*, 2011, pp. 156–162.

[3] A. Seth, J. L. Hicks, T. K. Uchida, A. Habib, C. L. Dembia, J. J. Dunne, C. F. Ong, M. S. DeMers, A. Rajagopal, M. Millard, S. R. Hamner, E. M. Arnold, J. R. Yong, S. K. Lakshmikanth, M. A. Sherman, J. P. Ku, and S. L. Delp, "OpenSim: Simulating musculoskeletal dynamics and neuromuscular control to study human and animal movement," *PLOS Comput. Biol.*, vol. 14, no. 7, Jul. 2018, Art. no. e1006223.

[4] K. R. Saul, X. Hu, C. M. Goehler, M. E. Vidt, M. Daly, A. Velisar, and W. M. Murray, "Benchmarking of dynamic simulation predictions in two software platforms using an upper limb musculoskeletal model," *Comput. Methods Biomech. Biomed. Eng.*, vol. 18, no. 13, pp. 1445–1458, Oct. 2015.

[5] L. Engelhardt, M. Melzner, L. Havelkova, P. Fiala, P. Christen, S. Dendorfer, and U. Simon, "A new musculoskeletal anybody detailed hand model," *Comput. Methods Biomech. Biomed. Eng.*, vol. 24, no. 7, pp. 1–11, 2020.

[6] S. Tata Ramalingasetty, S. M. Danner, J. Arreguit, S. N. Markin, D. Rodarie, C. Kathe, G. Courtine, I. A. Rybak, and A. J. Ijspeert, "A whole-body musculoskeletal model of the mouse," *IEEE Access*, vol. 9, pp. 163861–163881, 2021.

[7] S. L. Delp, F. C. Anderson, A. S. Arnold, P. Loan, A. Habib, C. T. John, E. Guendelman, and D. G. Thelen, "OpenSim: Open-source software to create and analyze dynamic simulations of movement," *IEEE Trans. Biomed. Eng.*, vol. 54, no. 11, pp. 1940–1950, Nov. 2007.

[8] M. S. Shourijeh, K. B. Smale, B. M. Potvin, and D. L. Benoit, "A forward-muscular inverse-skeletal dynamics framework for human musculoskeletal simulations," *J. Biomech.*, vol. 49, no. 9, pp. 1718–1723, Jun. 2016.

[9] H. Stark, M. S. Fischer, A. Hunt, F. Young, R. Quinn, and E. Andrada, "A three-dimensional musculoskeletal model of the dog," *Sci. Rep.*, vol. 11, no. 1, pp. 1–13, May 2021.

[10] K. R. S. Holzbaur, W. M. Murray, and S. L. Delp, "A model of the upper extremity for simulating musculoskeletal surgery and analyzing neuromuscular control," *Ann. Biomed. Eng.*, vol. 33, no. 6, pp. 829–840, Jun. 2005.

[11] J. L. Nuzzo, J. L. Taylor, and S. C. Gandevia, "CORP: Measurement of upper and lower limb muscle strength and voluntary activation," *J. Appl. Physiol.*, vol. 126, no. 3, pp. 513–543, Mar. 2019.

[12] T. Geijtenbeek, F. Steenbrink, B. Otten, and O. Even-Zohar, "D-Flow: Immersive virtual reality and real-time feedback for rehabilitation," in *Proc. 10th Int. Conf. Virtual Reality Continuum Appl. Ind.*, Dec. 2011, pp. 201–208.

[13] G. Durandau, D. Farina, and M. Sartori, "Robust real-time musculoskeletal modeling driven by electromyograms," *IEEE Trans. Biomed. Eng.*, vol. 65, no. 3, pp. 556–564, Mar. 2018.

[14] A. Patrick and K. Abdel-Malek, "A musculoskeletal model of the upper limb for real time interaction," SAE Tech. Paper 2007-01-2488, 2007, doi: 10.4271/2007-01-2488.

[15] A. J. van den Bogert, T. Geijtenbeek, O. Even-Zohar, F. Steenbrink, and E. C. Hardin, "A real-time system for biomechanical analysis of human movement and muscle function," *Med. Biol. Eng. Comput.*, vol. 51, no. 10, pp. 1069–1077, Oct. 2013.

[16] A. Murai, K. Kurosaki, K. Yamane, and Y. Nakamura, "Musculoskeletal-see-through mirror: Computational modeling and algorithm for whole-body muscle activity visualization in real time," *Prog. Biophys. Mol. Biol.*, vol. 103, nos. 2–3, pp. 310–317, Dec. 2010.

[17] Y. K. Tamilselvam, J. Ganguly, R. V. Patel, and M. Jog, "Musculoskeletal model to predict muscle activity during upper limb movement," *IEEE Access*, vol. 9, pp. 111472–111485, 2021.

[18] J. A. Barrios, K. M. Crossley, and I. S. Davis, "Gait retraining to reduce the knee adduction moment through real-time visual feedback of dynamic knee alignment," *J. Biomechanics*, vol. 43, no. 11, pp. 2208–2213, Aug. 2010.

[19] P. Teran-Yengle, R. Birkhofer, M. A. Weber, K. Patton, E. Thatcher, and H. J. Yack, "Efficacy of gait training with real-time biofeedback in correcting knee hyperextension patterns in young women," *J. Orthopaedic Sports Phys. Therapy*, vol. 41, no. 12, pp. 948–952, Dec. 2011.

[20] M. Sartori, M. Reggiani, D. Farina, and D. G. Lloyd, "EMG-driven forward-dynamic estimation of muscle force and joint moment about multiple degrees of freedom in the human lower extremity," *PLoS ONE*, vol. 7, no. 12, Dec. 2012, Art. no. e52618.

[21] B. M. Ashby and S. L. Delp, "Optimal control simulations reveal mechanisms by which arm movement improves standing long jump performance," *J. Biomech.*, vol. 39, no. 9, pp. 1726–1734, 2006.

[22] A. A. Saputra, J. Botzheim, A. J. Ijspeert, and N. Kubota, "Combining reflexes and external sensory information in a neuromusculoskeletal model to control a quadruped robot," *IEEE Trans. Cybern.*, vol. 52, no. 8, pp. 7981–7994, Aug. 2022.

[23] A. A. Saputra, C. W. Hong, A. J. Ijspeert, and N. Kubota, "A muscle-reflex model of forelimb and hindlimb of felidae family of animal with dynamic pattern formation stimuli," in *Proc. Int. Joint Conf. Neural Netw. (IJCNN)*, 2020, pp. 1–8.

[24] E. Todorov, T. Erez, and Y. Tassa, "MuJoCo: A physics engine for model-based control," in *Proc. IEEE/RSJ Int. Conf. Intell. Robots Syst.*, Oct. 2012, pp. 5026–5033.

[25] M. Damsgaard, J. Rasmussen, S. T. Christensen, E. Surma, and M. de Zee, "Analysis of musculoskeletal systems in the anybody modeling system," *Simul. Model. Pract. Theory*, vol. 14, no. 8, pp. 1100–1111, Nov. 2006.

[26] S. L. Delp and J. P. Loan, "A graphics-based software system to develop and analyze models of musculoskeletal structures," *Comput. Biol. Med.*, vol. 25, no. 1, pp. 21–34, Jan. 1995.

[27] D. J. Cleather and A. M. J. Bull, "The development of a segment-based musculoskeletal model of the lower limb: Introducing FreeBody," *Roy. Soc. Open Sci.*, vol. 2, no. 6, Jun. 2015, Art. no. 140449.

[28] F. C. T. van der Helm, "A finite element musculoskeletal model of the shoulder mechanism," *J. Biomech.*, vol. 27, no. 5, pp. 551–569, May 1994.

[29] A. Asadi Nikooyan, H. E. J. Veeger, E. K. J. Chadwick, M. Praagman, and F. C. T. van der Helm, "Development of a comprehensive musculoskeletal model of the shoulder and elbow," *Med. Biol. Eng. Comput.*, vol. 49, no. 12, pp. 1425–1435, Dec. 2011.

[30] S. Lee, M. Park, K. Lee, and J. Lee, "Scalable muscle-actuated human simulation and control," *ACM Trans. Graph.*, vol. 38, no. 4, pp. 1–13, Aug. 2019.

[31] S.-J. Chung and N. Pollard, "Predictable behavior during contact simulation: A comparison of selected physics engines," *Comput. Animation Virtual Worlds*, vol. 27, nos. 3–4, pp. 262–270, May 2016.

[32] T. Erez, Y. Tassa, and E. Todorov, "Simulation tools for model-based robotics: Comparison of bullet, Havok, MuJoCo, ODE and PhysX," in *Proc. IEEE Int. Conf. Robot. Autom. (ICRA)*, May 2015, pp. 4397–4404.

[33] J. H. de Groot and R. Brand, "A three-dimensional regression model of the shoulder rhythm," *Clin. Biomech.*, vol. 16, no. 9, pp. 735–743, Nov. 2001.

[34] G. Wu, F. C. T. van der Helm, H. E. J. D. Veeger, M. Makhsous, P. Van Roy, C. Anglin, J. Nagels, A. R. Karduna, K. McQuade, X. Wang, F. W. Werner, and B. Buchholz, "ISB recommendation on definitions of joint coordinate systems of various joints for the reporting of human joint motion—Part II: Shoulder, elbow, wrist and hand," *J. Biomechanics*, vol. 38, no. 5, pp. 981–992, May 2005.
[35] A. Ikkala and P. Hämäläinen, "Converting biomechanical models from OpenSim to MuJoCo," 2020, *arXiv:2006.10618*.
[36] K. R. S. Holzbaur, W. M. Murray, G. E. Gold, and S. L. Delp, "Upper limb muscle volumes in adult subjects," *J. Biomech.*, vol. 40, no. 4, pp. 742–749, 2007.
[37] K. R. S. Holzbaur, S. L. Delp, G. E. Gold, and W. M. Murray, "Moment-generating capacity of upper limb muscles in healthy adults," *J. Biomech.*, vol. 40, no. 11, pp. 2442–2449, 2007.
[38] M. Millard, T. Uchida, A. Seth, and S. L. Delp, "Flexing computational muscle: Modeling and simulation of musculotendon dynamics," *J. Biomech. Eng.*, vol. 135, no. 2, pp. 1–14, Feb. 2013.
[39] D. G. Thelen, "Adjustment of muscle mechanics model parameters to simulate dynamic contractions in older adults," *J. Biomech. Eng.*, vol. 125, no. 1, pp. 70–77, Feb. 2003.
[40] Y. Lee, M. S. Park, T. Kwon, and J. Lee, "Locomotion control for many-muscle humanoids," *ACM Trans. Graph.*, vol. 33, no. 6, pp. 1–11, Nov. 2014.
[41] Ł. Kidziński, S. P. Mohanty, C. F. Ong, Z. Huang, S. Zhou, A. Pechenko, A. Stelmaszczyk, P. Jarosik, M. Pavlov, and S. Kolesnikov, "Learning to run challenge solutions: Adapting reinforcement learning methods for neuromusculoskeletal environments," in *Proc. NIPS Competition, Building Intell. Syst.* Cham, Switzerland: Springer, 2018, pp. 121–153.
[42] K. Kaminishi, P. Jiang, R. Chiba, K. Takakusaki, and J. Ota, "Postural control of a musculoskeletal model against multidirectional support surface translations," *PLoS ONE*, vol. 14, no. 3, Mar. 2019, Art. no. e0212613.
[43] Y. Suzuki, T. Nomura, M. Casadio, and P. Morasso, "Intermittent control with ankle, hip, and mixed strategies during quiet standing: A theoretical proposal based on a double inverted pendulum model," *J. Theor. Biol.*, vol. 310, pp. 55–79, Oct. 2012.
[44] E. K. Chadwick, D. Blana, R. F. Kirsch, and A. J. van den Bogert, "Real-time simulation of three-dimensional shoulder girdle and arm dynamics," *IEEE Trans. Biomed. Eng.*, vol. 61, no. 7, pp. 1947–1956, Jul. 2014.
[45] A. A. Saputra, A. R. A. Besari, and N. Kubota, "Human joint skeleton tracking using multiple Kinect azure," in *Proc. Int. Electron. Symp. (IES)*, Aug. 2022, pp. 430–435.
[46] *Azure Kinect Body Tracking SDK, Microsoft*, Microsoft Development Team, Redmond, WAS, USA, 2021.
[47] J. C. Otis, C. C. Jiang, T. L. Wickiewicz, M. G. Peterson, R. F. Warren, and T. J. Santner, "Changes in the moment arms of the rotator cuff and deltoid muscles with abduction and rotation," *J. Bone Joint Surg.*, vol. 76, no. 5, pp. 667–676, May 1994.
[48] J. Liu, R. Hughes, W. Smutz, G. Niebur, and K. Nan-An, "Roles of deltoid and rotator cuff muscles in shoulder elevation," *Clin. Biomech.*, vol. 12, no. 1, pp. 32–38, Jan. 1997.
[49] R. E. Hughes, G. Niebur, J. Liu, and K.-N. An, "Comparison of two methods for computing abduction moment arms of the rotator cuff," *J. Biomech.*, vol. 31, no. 2, pp. 157–160, May 1997.
[50] D. K. Kuechle, S. R. Newman, E. Itoi, B. F. Morrey, and K.-N. An, "Shoulder muscle moment arms during horizontal flexion and elevation," *J. Shoulder Elbow Surgery*, vol. 6, no. 5, pp. 429–439, Sep. 1997.
[51] W. M. Murray, T. S. Buchanan, and S. L. Delp, "Scaling of peak moment arms of elbow muscles with upper extremity bone dimensions," *J. Biomech.*, vol. 35, no. 1, pp. 19–26, Jan. 2002.
[52] J. D. Webb, S. S. Blemker, and S. L. Delp, "3D finite element models of shoulder muscles for computing lines of actions and moment arms," *Comput. Methods Biomech. Biomed. Eng.*, vol. 17, no. 8, pp. 829–837, Jun. 2014.
[53] A. K. Bremer, G. R. Sennwald, P. Favre, and H. A. C. Jacob, "Moment arms of forearm rotators," *Clin. Biomech.*, vol. 21, no. 7, pp. 683–691, Aug. 2006.
[54] J. C. Ives and J. K. Wigglesworth, "Sampling rate effects on surface EMG timing and amplitude measures," *Clin. Biomech.*, vol. 18, no. 6, pp. 543–552, Jul. 2003.
[55] *Robot Assist Walker RT.1: Products: Rt.Works Co., Ltd.* Accessed: Jan. 19, 2023. [Online]. Available: https://www.rtworks.co.jp/eng/product/rt1.html

AZHAR AULIA SAPUTRA (Member, IEEE) received the B.A.S. degree in electronic engineering from Politeknik Elektronika Negeri Surabaya, Indonesia, in March 2014, and the M.E. and Ph.D. degrees from Tokyo Metropolitan University, Japan, in March 2018 and March 2021, respectively. Throughout his academic and professional career, he has achieved noteworthy milestones, including winning a Bronze Prize Award at the Capstone Design Fair International Session, South Korea, and garnering multiple victories in both national and international robotic competitions. From 2018 to 2021, he was a Ph.D. student at Tokyo Metropolitan University, participating in the JSPS Research Fellow—DC1 Program. In recognition of his research, he was honored with the Excellent Graduate School Research Award by the Japan Society of Automotive Engineers (JSAE), in 2020. He currently serves as an Assistant Professor at Tokyo Metropolitan University, focusing his research endeavors on intelligent control systems, neural-based locomotion systems, and robotics.

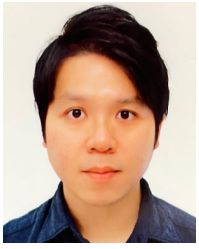

CHIN WEI HONG received the B.E. (Hons.) degree in robotics and automation from Multimedia University, Malaysia, in 2011, the master's degree in computer science from the University of Malaya, Kuala Lumpur, Malaysia, in 2015, and the Ph.D. degree from Tokyo Metropolitan University, Tokyo, Japan, in 2019. He is currently an Assistant Professor with the Department of Systems Design, Tokyo Metropolitan University. His current research interests include biologically-inspired robot navigation, lifelong machine learning, biologically-inspired robot mapping, and multimodal learning.

TADAMITSU MATSUDA (Member, IEEE) received the B.H.Sc., M.S., and Ph.D. degrees from Tokyo Metropolitan University, Tokyo, Japan, in 2004, 2006, and 2009, respectively. He joined Ryotokuji University, Chiba, Japan, as an Assistant, in 2007. He joined the Department of Physical Therapy, Uekusa University, Chiba, as a Lecturer, in 2012. He joined the Department of Physical therapy, Josai International University, Chiba, as an Associate Professor, in 2017. He joined the Department of Physical Therapy, Juntendo University, Chiba, an Associate Professor, in 2019. His focuses specifically on physical therapy, biomachanics, and rehabilitation engineering.

NAOYUKI KUBOTA (Member, IEEE) received the B.Sc. degree from Osaka Kyoiku University, Kashiwara, Japan, in 1992, the M.Eng. degree from Hokkaido University, Hokkaido, Japan, in 1994, and the D.E. degree from Nagoya University, Nagoya, Japan, in 1997.

He joined the Osaka Institute of Technology, Osaka, Japan, in 1997. He joined the Department of Human and Artificial Intelligence Systems, University of Fukui, Fukui, Japan, as an Associate Professor, in 2000. He joined the Department of Mechanical Engineering, Tokyo Metropolitan University, Hachioji, Japan, in 2004. He was an Associate Professor, from 2005 to 2012, and has been a Professor with the Department of System Design, Tokyo Metropolitan University, Tokyo, Japan, since 2012.